Chest Tomosynthesis for Detection and Surveillance of Pulmonary Pathology

Studies on Cystic Fibrosis and Solid Pulmonary Nodules

Carin Meltzer

Department of Radiology
Institute of Clinical Sciences
Sahlgrenska Academy, University of Gothenburg

UNIVERSITY OF GOTHENBURG

Gothenburg 2019

Cover illustration: A patient with Cystic Fibrosis and an example of a solid lung nodule depicted by conventional radiography, computed tomography and digital tomosynthesis.

Chest Tomosynthesis for Detection and Surveillance of Pulmonary Pathology
Studies on Cystic Fibrosis and Solid Pulmonary Nodules
© Carin Meltzer 2019
carin.meltzer@gu.se / camelt@ous-hf.no

ISBN 978-91-7833-474-2 (PRINT)
ISBN 978-91-7833-475-9 (PDF)
http://hdl.handle.net/2077/60286

Printed in Gothenburg, Sweden 2019
Printed by BrandFactory

This thesis is dedicated to the clinical and scientific community of diagnostic imaging.

Chest Tomosynthesis for Detection and Surveillance of Pulmonary Pathology

Studies on Cystic Fibrosis and Solid Pulmonary Nodules

Carin Meltzer

Department of Radiology, Institute of Clinical Sciences
Sahlgrenska Academy, University of Gothenburg
Gothenburg, Sweden

ABSTRACT

Introduction: Digital tomosynthesis (DTS) is a relatively new imaging modality in thoracic imaging. The technique is based on the equipment of conventional radiography, upgraded with a moving tube that enables separation of structures that are superimposed on chest x-ray (CXR). DTS has proven to be superior to CXR in detection of pathology, as well as a problem-solver for inconclusive findings in CXR, and has also been suggested as a low-dose / low-cost alternative to computed tomography (CT). However, the number of studies comparing DTS with CT are limited. Consequently, the overall aim of this thesis was to compare pulmonary imaging in DTS with CT, and to investigate the potential for DTS to serve as an alternative to CT. The performance of DTS was evaluated in terms of visualization, characterization, detection and follow-up of structural changes for two groups that often undergo multiple CT examinations; patients with cystic fibrosis (CF), and individuals with incidental solid pulmonary nodules.

Methods: Visibility of anatomical structures in CF was studied by a head-to-head comparison of concurrently performed CT and DTS (*Paper I*). Estimation of extent of disease was quantified by modality-specific scoring methods on CT, DTS and CXR, in two sets of examinations for each participant, separated by three years (*Paper II*).
The studies on pulmonary nodules were based on individuals recruited from the pilot study of the population-based Swedish CArdioPulmonary bioImage Study (SCAPIS), with incidental solid nodules requiring follow-up detected on

chest CT. Participants were examined by DTS in addition to routine CT for surveillance of nodule growth. Detection rates and recommendation for follow-up were independently assessed on DTS and compared to CT (*Paper III*). Nodule size and change of size between two examinations were estimated by diametrical measurements on DTS and semi-automated derived diameters and volume on CT (*Paper IV*).

Results: The studies on CF showed equal or superior visibility of anatomical structures in DTS in 48% of the cases. Structures in the anterior, posterior and lower parts of the lungs were less well depicted than those located in the central and lateral parts. Perceived visibility varied significantly among the observers (*Paper I*). Inter-modality correlation between DTS and CT for assessment of extent of disease was very strong regarding total severity score as well as sub-scores of bronchiectasis and bronchial wall thickening, which are key findings in CF (*Paper II*).
Nodule detection rates in DTS were between 48 and 62% for nodules measuring 5-10 mm in diameter, with a reduced number of nodules recommended for follow-up compared to CT (*Paper III*). An acceptable inter-modality agreement of average diameter, but lower agreement compared to volumetric estimates on CT was found (*Paper IV*).

In conclusion, the results indicate that DTS could be an alternative to CT in surveillance of patients with CF, and for follow-up of well-depicted solid nodules. Further studies including cases with progressive disease are warranted.

Keywords: Digital Tomosynthesis, Cystic Fibrosis, Solid Lung Nodules

ISBN 978-91-7833-474-2 (PRINT)
ISBN 978-91-7833-475-9 (PDF)

SAMMANFATTNING PÅ SVENSKA

Lungtomosyntes (LTS) är en röntgenmetod som ger en mer detaljerad avbildning av lungorna än traditionell lungröntgen, till lägre stråldos och kostnad än datortomografi (DT). DT leder till en relativt hög exponering för joniserande strålning, och med tanke på risken för strålinducerad cancer är det viktigt att minimera dosen för undersökningar som utförs upprepade gånger på samma individ. Patienter med sjukdomen cystisk fibros (CF) och individer med små runda förtätningar i lungorna (”noduler”), där det finns risk för lungcancer, är två grupper som ofta följs med upprepade DT. Denna avhandling utvärderar användning av LTS i dessa två patientgrupper.

Det första delarbetet jämför synbarheten av lungstrukturer i LTS och DT hos vuxna patienter med CF. Resultaten visar att synbarheten i cirka hälften av bedömningarna skattas sämre i LTS än i DT, särskilt i de främre, bakre och nedre delarna av lungorna. Det andra delarbetet jämför skattad grad av lungengagemang vid CF mellan lungröntgen, LTS och DT samt förmågan att påvisa förändringar i gradering av lungengagemang vid uppföljning med respektive metod. Resultaten visar överlag en god samstämmighet mellan undersökningsmetoderna.

I delarbete tre och fyra jämförs avbildning av noduler med LTS och DT. Deltagare i förstudien till befolkningsstudien ” the Swedish CArdioPulmonary bioImage Study”, hos vilka noduler som krävde uppföljning upptäcktes på DT, tillfrågades om undersökning med LTS i tillägg till planerad kontroll med DT. Resultaten från delarbete tre visar att ett lägre antal små noduler påvisas och rekommenderas för uppföljning med LTS jämfört med DT, samt att det finns en risk för feltolkning av misstänkta fynd med LTS. Delarbete fyra jämför bestämning av storlek och storleks-förändring av nodulerna mellan uppföljande undersökningar med LTS och DT, eftersom storlek och storleksförändring har en helt avgörande betydelse för vidare handläggning. Resultaten visar god överensstämmelse mellan manuella mätningar av noduldiameter på LTS och DT, men en sämre överensstämmelse mellan manuella mått på LTS och datorassisterad bestämning av nodulvolym på DT.

Slutsatsen är att LTS kan var ett stråldosbesparande alternativ till DT, men metoden har begränsningar vad gäller såväl påvisande som karakterisering av diskreta och små lungförändringar.

LIST OF PAPERS

This thesis is based on the following studies, referred to in the text by their Roman numerals.

I. Meltzer C, Båth M, Kheddache S, Ásgeirsdóttir H, Gilljam M, Johnsson Å A.
Visibility of structures of relevance for patients with cystic fibrosis in chest tomosynthesis: influence of anatomical location and observer experience.
Radiation Protection Dosimetry 2016;169(1-4):177-187.

II. Meltzer C, Gilljam M, Vikgren J, Norrlund RR, Vult von Steyern K, Båth M, Johnsson Å A.
Surveillance of pulmonary pathology in cystic fibrosis – comparison between digital chest tomosynthesis and computed tomography.
Submitted

III. Meltzer C, Vikgren J, Bergman B, Molnar D, Norrlund R R, Hassoun A, Gottfridsson B, Båth M and Johnsson Å A.
Detection and characterization of solid pulmonary nodules at digital chest tomosynthesis: data from a cohort of the pilot Swedish CArdioPulmonary bioImage Study.
Radiology 2018;287(3):1018-1027.

IV. Meltzer C, Fagman E, Vikgren J, Molnar D, Borna E, Beni M M, Brandberg J, Bergman B, Båth M, Johnsson Å A.
Surveillance of small, solid pulmonary nodules at digital chest tomosynthesis: data from a cohort of the pilot Swedish CArdioPulmonary bioImage Study
Submitted

CONTENTS

ABBREVIATIONS

AP	Antero-Posterior
ALARA	As Low As Reasonably Achievable
AUC	Area Under the Curve
BMI	Body Mass Index
CAD	Computer Aided Detection
CF	Cystic Fibrosis
CFTR	Cystic Fibrosis Transmembrane conductance Regulator
CI	Confidence Interval
CT	Computed Tomography
CTDI	Computed Tomography Dose Index
CXR	Chest X-Ray
DAP	Dose Area Product
DLP	Dose Length Product
DTS	Digital TomoSynthesis
HRCT	High-Resolution Computed Tomography
ICRP	International Commission on Radiological Protection
JAFROC	JAckknife Free-response Receiver Operating Characteristics
LOA	Limits Of Agreement
MRI	Magnetic Resonance Imaging
MRMC	Multiple-Reader Multiple-Case

PA	Postero-Anterior
PET-CT	Positron-Emission Tomography and Computed Tomography
PFN	Peri-Fissural Nodule
PRAGMA	Perth-Rotterdam Annotated Grid Morphometric Analysis
ROC	Receiver Operating Characteristics
ROI	Region Of Interest
SCAPIS	Swedish CArdioPulmonary bioImage Study
SD	Standard Deviation
SPN	Solid Pulmonary Nodule
Sv	Sievert (unit for effective dose)
VDT	Volume Doubling Time
VGC	Visual Grading Characteristics

1 INTRODUCTION

Diagnostic imaging plays a central role in medicine, with an increasing number of individuals undergoing screening, staging and surveillance of disease. Many organs and structures of the thorax are vital, complex and difficult to access, and imaging is a valuable tool for guiding for tissue samples and catheters, and anatomical orientation before invasive procedures. The main modalities for imaging of the lungs are conventional chest radiography (CXR) and computed tomography (CT). Positron emission tomography-computed tomography (PET-CT) is standard in many regimes for cancer staging and magnetic resonance imaging (MRI) is gradually finding its place for some clinical tasks.

The American Food and Drug Administration (FDA) approved digital tomosynthesis (DTS) for diagnostic imaging in 2005, and studies and clinical experience report superior diagnostic precision compared to CXR. DTS could be a low-cost/low-dose alternative to CT, but the knowledge regarding performance and potential clinical impact is limited. Consequently, this thesis concern clinical validation of DTS compared to CT for imaging of patients with cystic fibrosis and individuals with lung nodules, two groups that would potentially benefit from the modality as an alternative to CT.

2 BACKGROUND

2.1 MODALITIES FOR THORACIC IMAGING

CONVENTIONAL RADIOGRAPHY

The German mechanical engineer, physicist and professor Wilhelm Conrad Röntgen discovered a new type of radiation in 1895 [1] known as X-rays, an intervention that was awarded with the Nobel Prize in 1901. The electromagnetic radiation travels through the body, producing an image based on the amount of energy that reaches the detector behind the object, which is depending on the density of the body parts. The first clinical implications were mainly fractures and localization of foreign bodies. As the imaging technique was further improved, it became an increasingly valuable asset in patient care. The conversion from analog to digital technique around year 2000 is the most important recent development of the technique [2], which facilitated communication of images, optimization of image quality and radiation dose, as well as the ability for simulation of dose reduction and combination of clinical images with phantom lesions for study purposes.

Chest X-ray is a commonly performed radiological examination, providing an overview of the lungs, ribs, pleura and cardiovascular system. Standard imaging is performed with a postero-anterior (PA) and lateral view with the patient in standing position during a breath hold in full inspiration, exposing the patient to an effective dose below 0.1 mSv. The portable units also enable imaging of instable, severely ill patients, often examined in lying position with an antero-posterior (AP) view. Common reasons for request of a CXR are dyspnea, suspicion of infectious, inflammatory, or traumatic pathology, position of medical equipment, and to rule out large intrathoracic masses.

COMPUTED TOMOGRAPHY

Sir Godfrey Hounsfield [3] was an English electrical engineer, and his team contributed to the development of CT imaging, a method based on the idea that multiple X-rays projections in different angles of an object could be reconstructed to slice images. The first images of a patient was obtained by the prototype EMI head scanner, at the Atkinson Morley Hospital, London in 1971 [4]. The scanning technique became available to other hospitals during the following years, and the modality grew into a revolution in medical imaging. In addition to slice images, CT also enabled quantitative estimate of tissue density, known as "Hounsfield units". The first examinations were performed with transaxial technique directed at right angles to the long axis of the body. The step-and-shoot technique involves a full 360° rotation of the tube before the bed position is moved and a new rotation is performed. This technique provides high resolution images in one plane. Further development of the tube and detector made way for the helical technique around year 1990, with shorter scan time and possibility for multi planar image reconstructions [5]. Illustrations of transaxial and helical techniques are presented in Figure 1.

CT with or without contrast media is the reference modality for depiction of pathology in the thorax; in the parenchyma, airways, vessels as well as the pleura and mediastinum. A high-resolution computed tomography (HRCT) protocol is often used for a detailed visualization of the lung parenchyma, such as disease affecting the small airway, or pulmonary fibrosis [6].

Radiation exposure is the main concern regarding CT, and optimization of equipment and scan protocols has made way for parenchymal low-dose protocols at levels comparable to CXR [7, 8]. However, the effective dose for a standard helical chest CT is often between 1 and 10 mSv.

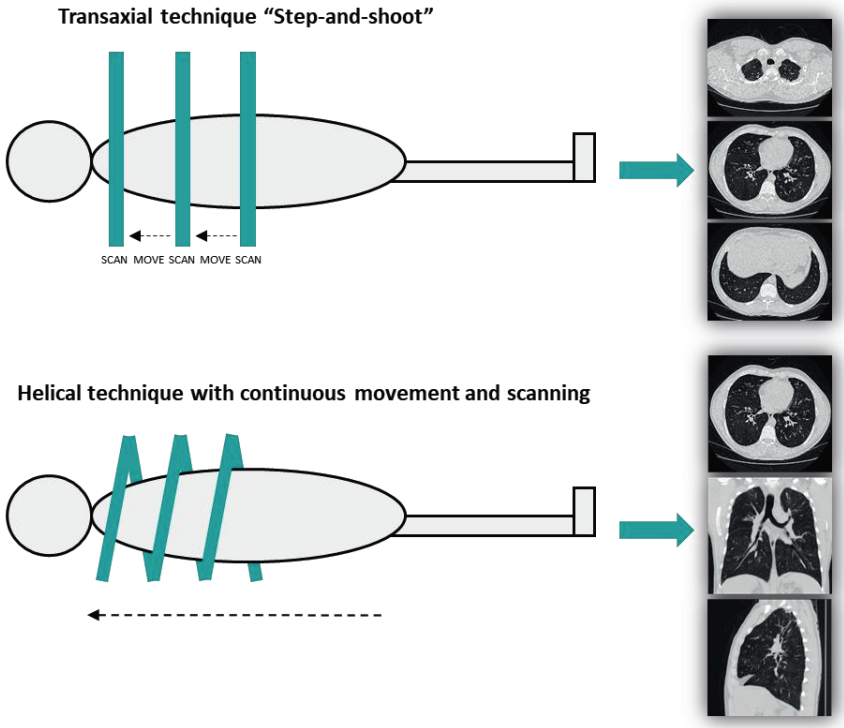

Figure 1. The transaxial technique provides images in the transverse plane, structures positioned between the scans are not visualized. The helical technique cover the whole volume and enables reconstruction of slice images in multiple planes.

POSITRON-EMISSION TOMOGRAPHY-COMPUTED TOMOGRAPHY

The interest and development of radiotracers began in early 1900, and the collaboration between several researchers led to the development of flurodeoxyglucose (^{18}F), a clinically tolerable isotope with acceptable half-life, first tested in humans 1976 [9]. Cells with high consumption of glucose, such as those affected by inflammation, infection and malignancy stand out with a high signal on the PET scan. The need for anatomical location of these areas made way for a combined examination of PET and low-dose CT, known as PET-CT, introduced in 2001 [10]. PET-CT is now a standard regime in characterization of suspicious lesions and staging of many types of cancer, including lung cancer. Some malignancies, such as carcinoids can have normal uptake of FDG, but other traces are available [11].

ULTRASOUND

Ultrasound provides images of internal organs based on high-frequency sound waves, and diagnostic images has been available since around World War II [12]. Ultrasound is non-radiating, easy accessible and portable. The main implications in the thoracic region are assessment of pleural effusion, pneumothorax, cardiac function and morphology and vascular flow. It is also the main modality for guiding in interventional procedures in vessels, pleura, lymph nodes and masses. The transmission of ultrasound waves is impaired in air and bones, and normal lung parenchyma and objects surrounded by aeriated structures are consequently less well depicted. However, ultrasound can be used to identify conditions with decreased aeration of parenchyma, such as atelectasis [13] and pulmonary edema [14].

MAGNETIC RESONANCE IMAGING

Magnetic Resonance Imaging (MRI) [15] is a non-radiating modality, where magnetic fields and radio waves are used to generate diagnostic images and the first human was examined in 1977. The technique is based on signals from protons in tissue, and is an established modality for cardiac and vascular imaging in clinical practice. The combination of low proton density, respiratory motions and artefacts in the interface between air and tissue has until recently limited the use of MRI in depiction of lung parenchyma. However, the superior visualization of soft-tissue and inflammation/edema without the use of intravenous contrast, ability for dynamic imaging as well as the avoidance of radiation exposure, in combination with technological development in terms of new and fast imaging sequences have now made way for MRI as an interesting alternative for imaging of the respiratory system [16, 17]. The use of hyperpolarized gas in MRI is a promising technique for visualization of ventilation [18].

DIGITAL TOMOSYNTHESIS

DTS [19, 20] is based on the equipment of conventional radiography, upgraded with a moving tube and special software. The angular movement of the tube enables separation of overlapping anatomy, otherwise superimposed on CXR. The considerable improvement in detection and characterization of pathology, with only a modest increase in radiation exposure compared to conventional radiography has led to a variety of suggested clinical implications for DTS [21]. DTS in breast imaging has already proved valuable, with a superior performance in detection of early cancer compared to the conventional mammogram, and DTS is now increasingly replacing mammography for routine breast cancer screening [22, 23]. Previous studies have shown superior performance of DTS compared to conventional radiography in imaging of the spine [24, 25], fractures [26, 27], and lungs [28-33], and the technique has also been suggested as an alternative to CT [29, 34, 35]. DTS is less time consuming regarding both image acquisition and reading, and contribute to radiation exposure substantially lower than for CT.

In DTS of the chest, the tube performs a caudo-cranial sweep ± 15° around the standard PA plane, collecting approximately 60 low-dose projections during 10-12 seconds. Imaging parameters are based on the signal from an initial low-dose scout image. Imaging acquisition in CXR and DTS is illustrated in Figure 2.

The low-dose projections are reconstructed to approximately 60 section images in the coronal plane, with a reconstruction interval of 5 mm. The slices are similar to coronal CT images, but with the difference that structures that lie in the focus plane are clearly depicted, and structures outside the plane are blurred. The resulting images have the same, high spatial resolution as CXR, which is superior to CT. There are, however, some drawbacks compared to CT; the limited angular movement of the tube leads to an inferior depth resolution, and detection and characterization of small structures can be difficult, especially in dense regions in the anterior and posterior aspects of the lungs [36-38]. Imaging examples are presented in Figure 3. Until recently, most studies have involved comparison between DTS and CXR, and the number of clinical studies with concurrently performed DTS and CT are limited.

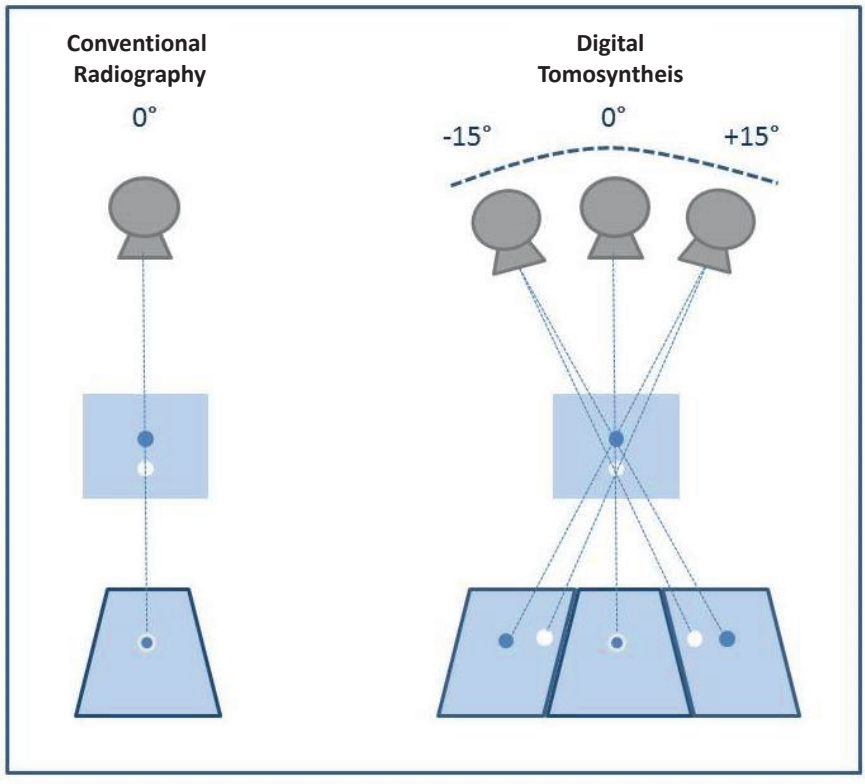

Figure 2. The angular sweep of digital tomosynthesis separates overlapping structures, otherwise superimposed on conventional radiography.

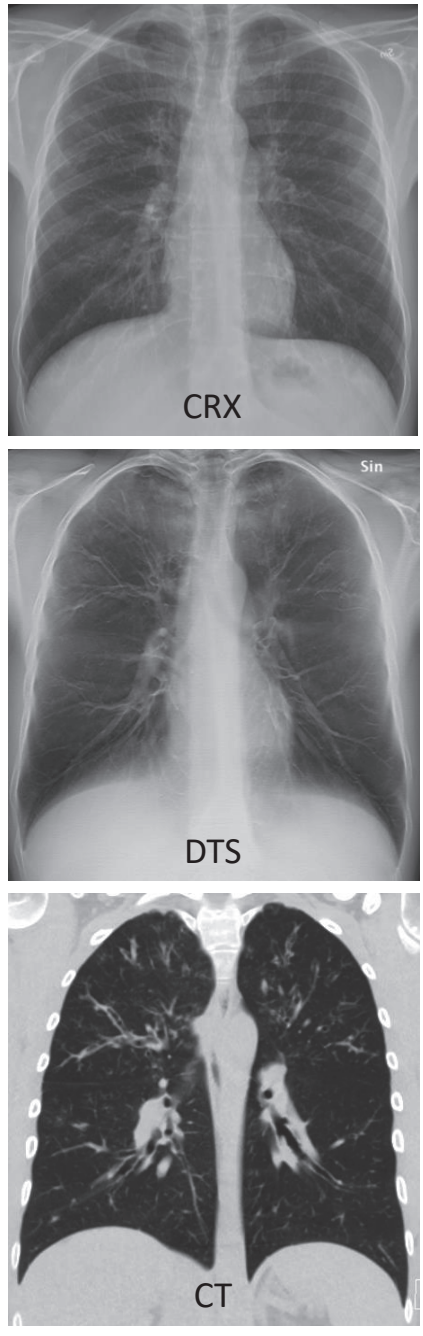

Figure 3. Example of CXR, DTS, and coronal CT of the same patient.

2.2 CYSTIC FIBROSIS

PATHOGENESIS AND CLINICAL ASPECTS

CF [39] is a genetic disorder caused by mutations in the cystic fibrosis transmembrane conductance regulator (CFTR) protein, inherited in an autosomal recessive manner. There are over 1,700 CF mutations, a comprehensive register is found in the CFTR-2 database (http://www.CFTR2.org), the most common being the F508del variant. Clinical symptoms require mutation in both gene copies, and individuals with only one mutation are carriers of the disorder. CF mutations affect either the CFTR protein or the CFTR channel, with a resulting defect in transmembrane transport of chloride and bicarbonate. The normal, thin mucus of the epithelial wall of the airways facilitates the clearance of inhaled particles and infectious agents, and CF mutations lead to a pathological thickening of mucus. More recent studies also suggest that the mutations have a direct effect on the immune-response, especially for infections with *Pseudomona aeruginosa* [40, 41].

The clinical symptoms of CF depend on the type of mutation, from non-symptomatic to lethal disease. The thick mucus forms plugs, mainly affecting the sinuses, lungs, pancreas, liver, digestive system and reproductive organs. CF can present with acute symptoms as with meconium ileus in a newborn, or a more chronic, progressive disease with malabsorption, infections and respiratory symptoms. Most patients require life-long follow-up at a multidisciplinary team, preferable at a dedicated CF center. Symptomatic treatment involves inhalations and physical therapy in order to aid the clearing of thick mucus of the airways, antibiotics for bacterial and fungal infections, and replacement therapy for pancreatic insufficiency. Potent, though expensive, CFTR modulator therapies are now available for some of the mutations. The combination of prophylactic and aggressive symptomatic treatment has improved the life expectancy considerable during the last decades [42].

Respiratory failure is the main cause of CF-related mortality. Mucus plugging in the airways initiates an inflammatory reaction, often further complicated by acute and chronic infections. Early detection and treatment of complications can prevent some of the irreversible structural changes, and surveillance with lung function tests, clinical examination, blood samples and radiological imaging are consequently recommended as standard of care. Quantification of

pulmonary involvement in CF is a challenging task due to the heterogeneity in type and distribution of pathology, though the images provide important information for the clinicians, especially when it comes to evaluation of the effect of CFTR modulator therapy. Examples of CT images of mild and severe structural lung disease in CF are presented in Figure 4.

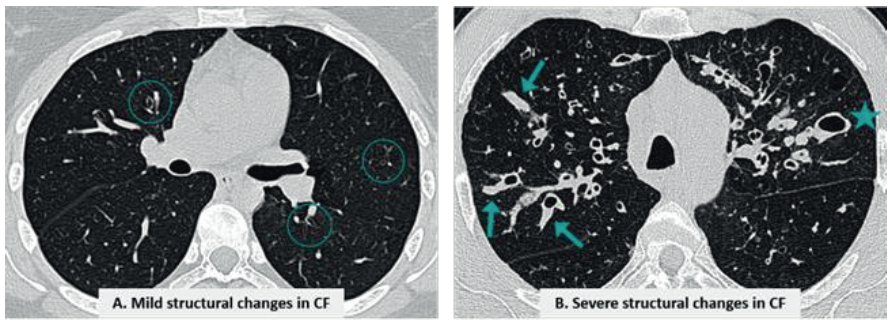

Figure 4. Examples of surveillance of two patients with CF. Transverse section image in a patient with mild disease (A) show a small number of cylindrical bronchiectasis with marked wall. More severe, partly irreversible changes are visible in patient B, with thick-walled and mucus filled bronchi (⇧), and a cystic bronchiectasis (★).

IMAGING OF CYSTIC FIBROSIS

Guidelines and clinical routines

The 2018 guidelines from European Cystic Fibrosis Society (ECFS) on monitoring of CF lung disease state: “Chest X-rays are routinely performed on an annual basis in most CF centers as well as at times of clinical deterioration. Other imaging modalities, such as high resolution CT scanning, should be available as well, and are used routinely in some CF centers” [43]. The Adult Care Clinical Care Guidelines from the Cystic Fibrosis Foundation from 2004[44] recommend CXR every 2-4 years in patients with stable clinical status, and that imaging is considered for patients with acute symptoms. Imaging surveillance is often performed according to local routines, and the combination of annual CXR and bi- or triannual CT is a common regime in the western world, but the radiation exposure associated with repeated CT in this young patient population is a concern.

Modalities for depiction of CF-related pulmonary pathology

Patients with CF have a broad spectrum of pulmonary pathology. Acute complications such as pneumonia and pneumothorax can be identified on CXR, but the complex, chronic changes can require alternative modalities for adequate visualization and characterization. CT is the most sensitive method for assessing the lung parenchyma, since it can reveal both subtle, early changes such as thin-walled bronchiectasis, as well as small areas with severe focal disease, which is an important finding, especially in cases where clinical symptoms, lung function test and blood samples are normal or unchanged [45-47]. HRCT was previously performed by step-and-shoot technique due to sharper contrast in the images at lower radiation doses than helical CT. Developments in the CT technique have improved the resolution and decreased the radiation exposure for helical scans. Today, HRCT images are mainly achieved by reconstruction of thin section transverse images with a sharp filter from a helical scan, with the advantage of assessment in additional multi planar reconstructions and less respiratory artefacts.

MRI, DTS and FDG PET-CT are undergoing evaluation as additional or alternative modalities for chest imaging in CF. MRI appears to be comparable to CT in some aspects, and provide additional information regarding the inflammatory activity in pathological changes [48]. MRI is implemented in the standard CF follow-up regimen for children at Sophia Children Hospital, Rotterdam, the Netherlands. Vult von Steyern *et al.* [49] and Gunnell *et al.* [50] have both shown that DTS is superior to CXR in pulmonary CF imaging, and DTS is the routine modality for CF surveillance at Department of Pediatric Radiology, Skåne University Hospital, Sweden.

Structural pulmonary changes in CF

Pathology related to CF can affect the whole airway system, which consists of the trachea, main bronchi, lobar bronchi, segmental bronchi, subsegmental bronchi and terminial bronchioles, which lead out to the alveoli where the gas-exchange takes place. The next section covers the key pulmonary findings in CF, and the ability of detection and characterization in diagnostic imaging.

Bronchiectasis: Bronchiectasis is a central pathological change in CF, defined as a pathological increase in bronchial diameter, either as 1; a ratio >1 between the diameter of a bronchi and the accommodating artery, 2; lack of tapering of

bronchial diameter, or 3; a visible bronchi within 1 cm of the pleural surface [51]. Bronchiectasis is a key finding in CF and closely related to overall pulmonary involvement and probability for acute exacerbation in CF [52]. An example of a normal and widened bronchi in CT is presented in Figure 5.

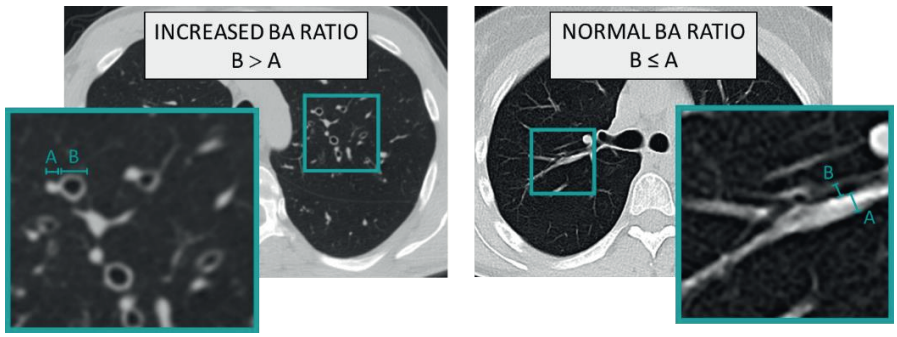

Figure 5. Transverse CT images of two patients with CF, one with normal BA ratio (right), and one with increased broncho-arterial (BA) ratio (left) consistent with cylindric bronchiectasis.

Bronchiectasis are closely related to overall pulmonary involvement and probability for acute exacerbations in CF [52], and are further characterized by shape as either cylindric (Figure 5), varicose or cystic (✶ Figure 4). A study by van der Bruggen-Boogarts *et al.* [53] regarding the performance of CXR in screening of bronchiectasis showed a 87.8% sensitivity and 74.4% specificity, having HRCT as reference, and a linear relationship between the extent of bronchiectasis on HRCT and abnormities on CXR. Sanders *et al.* [54] examined a pediatric CF-population with CXR and CT, and found a sensitivity of 91% in positive scoring for CT-verified bronchiectasis on CXR, though CXR was performed up to 1 year prior to CT. Several studies have shown good agreement between MRI and CT in detection of central bronchiectasis [55-57] but a lower sensitivity for MRI in visualization of peripheral bronchi. Visibility and characterization of bronchiectasis in DTS is superior to CXR [49], but the visibility compared to CT has not been reported.

Bronchial wall thickening: Bronchial wall thickening or peri-bronchial thickening is a key finding in CF, caused by infection and inflammation. Pathological wall thickening is defined as 1) bronchial wall thickness >2 mm in the hila, >1 mm in the central lung, or >0.5 mm in the peripheral lung, 2) total diameter of bronchial wall thickness × 2 exceeding the internal bronchial diameter, or 3) a ratio between arterial diameter and bronchial wall thickness >0.33 [58]. Bronchiectasis with thick walls can be seen as “tram track sign” on

CXR, but is often obscured due to overlapping anatomy. HRCT is the reference standard, but currently available MRI sequences enable visualization of edema in the bronchial wall, which gives important information regarding active inflammation vs chronical changes [56, 57, 59, 60]. Wall thickening in CF is often seen in combination with dilated bronchi, an example of bronchial wall thickening in DTS and CT in a patient with CF is presented in Figure 6.

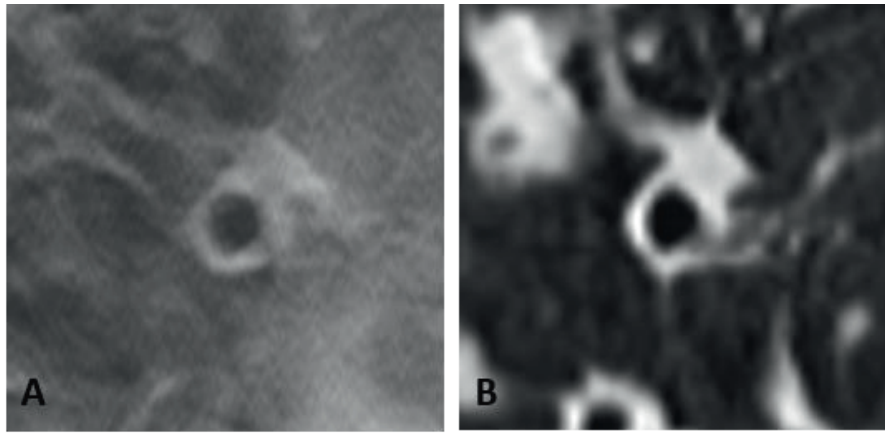

Figure 6. Bronchial wall thickening in a patient with cystic fibrosis depicted by A) DTS and B) CT.

Mucus plugging: Stagnation of thick mucus "mucus plugging" in central airways can be detected with CXR, DTS, CT and MRI. More peripheral plugging, known as "tree-in-bud" can be difficult to identify on CXR. An illustration is given in Figure 7.

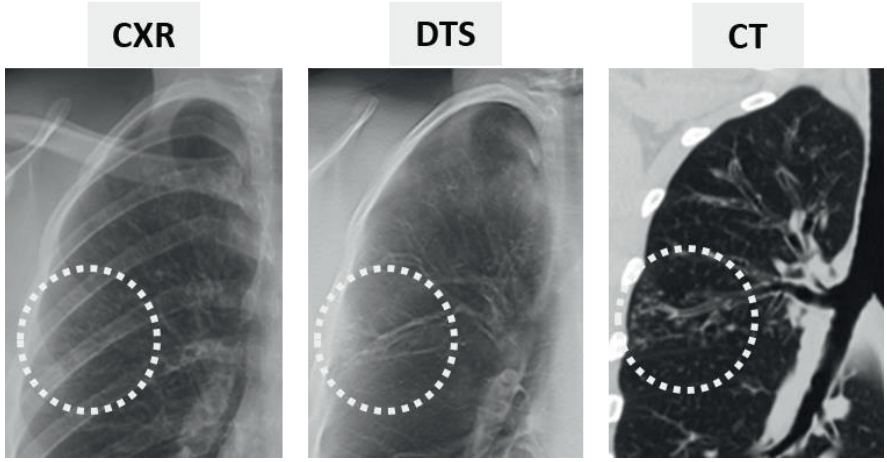

Figure 7. Mucus plugging in peripheral airways with a "tree-in-bud" pattern in a patient with cystic fibrosis examined by CXR, DTS and CT.

Collapse/consolidation: Parenchymal areas with increased density can have different causes such as infection, atelectasis and fibrosis. Findings of traction bronchiectasis and volume reduction is suggestive of chronical changes, but other opacities can be more difficult to characterize. Consolidation and the relation to the bronchial tree is well depicted on CT, and T2-weighted MRI can visualize edema as a sign of an active inflammatory process. The extent and relations of a parenchymal consolidation can be difficult to assess on CXR and DTS, and can be affected by anatomical location [36, 61].

Hyperinflation and airtrapping: Mosaic pattern is seen in conditions affecting the airways "airtrapping", and pulmonary vessels "regional differences in perfusion", traditionally separated by adding an expiratory scan to the standard inspiratory CT. These changes are however now considered closely related due to the mechanism of vasoconstriction of hypoventilated areas. Airtrapping is an important finding in CF, but can currently only be adequately visualized on CT. MR perfusion can visualize regional hypoperfusion, and gas-enhanced MRI is currently undergoing validation for

imaging of both hypoventilation and hypoperfusion [60, 62-64]. Hyperinflation is related to the obstructive components of CF, typical radiological features are flattened hemidiafragmatic contours, increased retrosternal space, hyperlucent lungs with increased volume, and increased anteroposterior diameter of the chest. The typical sign of hyperinflation is visible on both CXR and CT. DTS in clinical practice does not always include a lateral projection due to radiation consideration, which can impair the ability of assessment in some degree. The low proton density and thereby loss of MRI signal in lung parenchyma with reduced density makes it difficult for direct visualization of normal aeriated lung parenchyma, but hyperinflation is closely associated with reduced diaphragmatic movement and perfusion, which can be well visualized on cine and perfusion MRI sequences [48].

Scoring systems in CF

Quantification of structural pulmonary changes in CF is of importance in the evaluation of disease progression and response to treatment, especially for patients who receive CFTR modulation therapy, which comes at a high price and with potential side effects.

The first CF scoring systems was developed for CXR, and some of the most commonly used are the Chrispin-Norman score [65], Wisconsin score [66], Brasfield score [67] and Northern score [68]. All of these scoring systems have shown good correlation with clinical parameters and pulmonary function tests [69], despite suboptimal visualization of some of the pathological changes that are visible in CT. The Northern score is based on the PA projection only. Scoring is fast and can be performed after a short training session, and the system has been proven robust with high interobserver agreement [68]. Each lung is separated into an upper and lower zone, and the four quadrants is given a rating between 0 (normal) and 4 (very severe: little or no area of normal lung seen, dense infiltration), with a total score of 0-20.

More complex scoring systems have been developed for CT [70], with reproducible results and good correlation with lung function tests. The CF-CT scoring system is one of the most used, and it can be performed on both transaxial and helical CT scans [71]. The method requires a period of training and includes scoring of central and peripheral bronchiectasis, airway wall thickness, central and peripheral mucus plugging, parenchymal opacities, cyst and bullae and air trapping. The more recently developed Perth-Rotterdam Annotated Grid Morphometric Analysis (PRAGMA) method requires a helical

CT scan, and involves assessment of the whole lung volume. The main strength of the PRAGMA-score is the ability to assess discrete, early pathology in small children, as well as a high inter- and intraobserver agreement [72, 73], but the scores has the disadvantage that only the most severe type of pathology in a region is included in the analysis.

The differences in depiction of CF pathology between CT and MRI, especially of peripheral thin-walled bronchiectasis and air trapping induce the need for specific MRI scoring systems. Potential scoring systems are still undergoing clinical validation, but studies have so far shown good correlation with clinical parameters [56, 57, 59].

2.3 PULMONARY NODULES

ETIOLOGY AND IMAGING CHARACTERISTICS

A pulmonary nodule is defined as a rounded, up to 3 cm large opacity in the lung [51]. Small nodules are reported as incidental findings in 14-50% [74, 75] of individuals undergoing chest CT. Most nodules are benign with a broad variety of causes such as a granuloma after a previous infectious or inflammatory process, or an active process due to infection, inflammation or neoplasm. The most common benign nodules in the lungs are hamartoma and fibroma, and the main malignant lesions are primary lung cancer, lymphoma, carcinoid, sarcoma and metastasis.

The appearance of a nodule is of outmost importance when the radiologist tries to understand the nature of the lesion. Some nodules can be safely classified as benign when first detected, for example a fat-attenuating lesion with popcorn-like calcification consistent with a hamartoma, or a completely calcified nodule, often seen as the end-stage of a collection of inflammatory cells which goes under the term “granuloma”. Another important characteristic is the density of the nodule, where the dense, solid nodules completely obscure the bronchial and vascular margins of the underlying lung parenchyma. Ground glass nodules are less dense with visible underlying structures, and multiple ground glass nodules are often due to infection or inflammation. Semisolid nodules have both solid and ground glass components and these features should raise the suspicion of malignancy [76].

The distribution of the nodules is also of importance, a perilymphatic distribution along fissures, septa and adjacent to bronchovascular structures is typical for sarcoidosis, while a centrilobular, patchy pattern is more commonly seen in pathology affecting the airways.

There is an important distinction between parenchymal and peri-fissural nodules (PFNs): a typical PFN is a solid, triangular or lentiform, well-defined nodule located adjacent to pleura or fissures [77]. PFNs are often considered as intrapulmonaly lymph nodes. Ahn *et al*. [78] found PFNs in 67% of patients undergoing lung cancer screening, and a study by Mets *et al*. [79] showed a 26% prevalence of PFNs in a cohort of patients with and without incident lung cancer. Despite significant growth in some of the PFNs in both studies, none turned out to be malignant during follow-up, but PFN ≥10 mm can be

considered for further management as suggested for enlarged lymph nodes [76]. Examples of a SPN and a PFN are given in Figure 8.

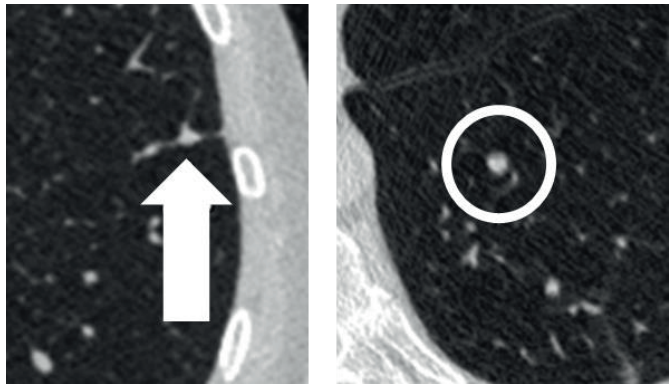

Figure 8. The left CT image with a triangular, subpleural nodule with strikes to the adjacent pleura, attributes consistent with a typical perifissural nodule (arrow). The right image with a solid, round opacity in the lung parenchyma consistent with a solid pulmonary nodule (circle).

SIZE ESTIMATES OF SOLID NODULES

Guidelines from the Fleishner Society [80] recommend manual measurements with electronic calipers of nodules on thin-section (1.5 mm or less) CT images, and reporting of the average of the longest diameter and the diameter perpendicular to this measurement, rounded to the nearest millimeter. An example of a manual size estimate is presented in Figure 9.

Figure 9. Thin-section transverse CT image of an incidental, solid nodule in the right upper lobe. Longest manually measured diameter (A) was 6.0 mm and perpendicular diameter (B) 4.5 mm. Reported average diameter is 6 mm (6+5/2=5.5, rounded to nearest diameter). Volumetric, semi-automated estimate was 66 mm^3.

There are several studies and guidelines that apply the longest nodule diameter, which is also used in the American Joint Committee on Cancer Staging Manual (www.cancerstaging.org), and in the Response Evaluation Criteria in Solid Tumors (RECIST) [81], both with widespread use worldwide. The reason for implementation of average diameter in manual size estimates of small nodules is an often better correlate to volume. Two retrospective studies on individuals undergoing lung cancer screening showed a reduction of false-positive lung nodules [82, 83] when applying average instead of maximum nodule diameter. The expected inter- and intraobserver variation on manual measurements is up to 1.7 mm, according to the results from Revel *el al.* [84].

The guidelines from the British Thoracic Society [85] recommend volumetry as the preferred measurement method. Manual measurement is an alternative method if volumetry is unavailable or technically impossible. Today, there are designated softwares that perform nodule detection (CAD) as well as volumetric estimate of nodule size in an automated or semi-automated process. The semi-automated method involves confirmation of suspected nodules by the radiologist, and correction of the contour in cases when the software is unable so separate the nodule from adjacent structures. Diameters and volume

are estimated based on a certain pixel value threshold, and the accuracy of the segmentation is dependent on software, image-acquisition, reconstruction algorithm, density, shape and location of the nodule. Variations in volume up to 25% [86, 87] can be expected for clinical nodules. An example of a segmented nodule is presented in Figure 10.

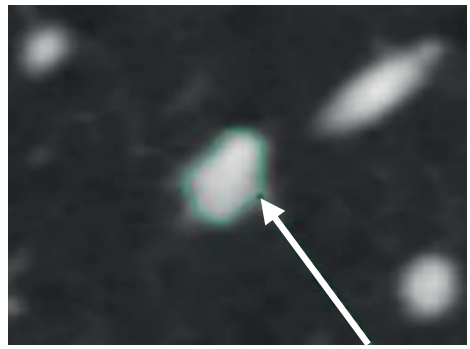

Figure 10. Semi-automated segmentation of a solid nodule on CT, size estimated as 8.0 x 5.5 mm and 159 mm^3.

MANAGEMENT OF SOLID NODULES

The size and growth of solid pulmonary nodules (SPNs) are positively related to the risk of malignancy, and therefore central in the decision for further work-up. Regional and international guidelines, such as those from the Fleischner Society [76] and the British Thoracic Society [85], provide evidence-based recommendations on management of incidental pulmonary nodules.

The Fleischner Society recommends surveillance for indeterminate nodules, defined as nodules with an estimated 1% or more risk of malignancy, which correspond to solid nodules with a diameter between 6 and 8 mm, or a volume between 100 and 250 mm^3. Nodules>8 mm should be considered for a 3-month follow-up or further work-up with PET-CT and/or biopsy due to a higher risk of malignancy. The 2017 guidelines [76] increased the minimum threshold to 6 mm from the previous 4 mm in the 2005 guidelines [88], mainly based on new knowledge from the lung cancer screening trials [89-91].

The British Thoracic Society [85] recommends routine follow-up of nodules with a volume ≥80 mm^3 or maximum diameter ≥5 mm three months after

baseline CT, and PET-CT for nodules with an initial risk of malignancy> 10% and size greater than the threshold for PET-CT.

ESTIMATION OF NODULE GROWTH

Growth is the key finding in indeterminate nodules, and the recommended time to first follow-up of solid nodules varies from 3 to 12 months [76, 85]. Nodule growth can be expressed as an increase in absolute diameter, a relative change in volume, or as volume doubling time (VDT). VDT represent the number of days for volumetric increase of 100%, and the equation includes an assumption of linear growth between the two examinations

The Fleishner Society recommends a minimum 2 mm difference in average, rounded diameter in manual measurements before a change in nodule size should be reported [80]. Volumetric estimates have shown to be superior to manual measurements in detection of nodule growth on CT [92-95], and should be performed with identical software versions with ideally the same imaging protocol and reconstruction algorithm on baseline and follow-up. The British Thoracic Society guidelines recommend a 25% cut-off for significant growth based on volumetric estimates [76].

The highest sensitivity for detection of malignant growth is achieved by estimation of VDT ([85]. Nodule volumes and VDT can be estimated from manual diameters in cases when volumetry is not available. The study from Henschke *et al.* [96], based on the International Early Lung Cancer Action Program found that all solid, nodular lung cancers had VDT <400 days. The British Thoracic Society Guidelines [85] recommends further work-up of solid nodules with VDT <400 days, consideration of biopsy or further CT surveillance for nodules with VDT 400-600 days, and discharge when VDT is >600 days. These recommendations do not apply for subsolid nodules, where malignancies can be more slowly growing with longer VDT, hence the need for a prolonged period of surveillance for up to 5 years. Examples of different methods for estimation of size and growth are presented in Table 1.

	Case 1	Case 2
Baseline CT		
Maximal diameter (mm)	6.0	6.2
Perpendicular diameter (mm)	4.5	4.8
Average diameter (mm)	6	6
Semi-automated volumetry (mm^3)	66	81
Follow-up CT		
Maximal diameter (mm)	7.0	7.2
Perpendicular diameter (mm)	4.5	5.9
Average diameter (mm)	6	7
Semi-automated volumetry (mm3)	87	139
Change in averge diameter (mm)	0	1
Change in semi-automated volumetry (mm^3)	21	58
Relative change in semi-automated volumetry (%)	+31.8	+70.0
VDT* based on semi-automated volumetry (days)	916 days	477

*Table 1. Case 1 shows a nodule with a 1 mm increase in longest diameter and a corresponding 31.8% increase in volume. The average diameter is however unchanged, and VDT is consistent with a benign lesion. Case 2 is an example of a small increase in both diameters, and a 70.0% increase in volume. The VDT is in the range 400-600 days, where ongoing surveillance or biopsy is recommended according to guidelines from the British Thoracic Society. Note that there is no significant change in average diameter (<2 mm). *Volume-doubling-time (VDT) with 365 days between baseline and follow-up.*

IMAGING OF PULMONARY NODULES

Conventional radiography

CXR was the standard modality for chest imaging for a long period, but visualization of nodules is dependent on anatomical location, density and size, and the inferior detection rate of small and subsolid lesions made way for the change to CT [97, 98]. CXR is also associated with considerable interobserver variation and indeterminate or false-positive findings [97]. Results from a randomized controlled trial involving 154,901 participants randomized to annual screening with CXR or usual care showed no effect on lung cancer mortality through the 13 years of follow-up [99]. However, the Fleischner Society guidelines [76] suggest that CXR may be a low dose / low cost

alternative for follow-up of clearly visualized nodules with a low risk of malignancy.

Computed tomography

CT is the current reference modality for detection, measurement and classification of nodules, with the additional advantage of CAD and segmentation. The main drawbacks of CT are radiation exposure, reading time, cost, in some cases accessibility, as well as the risk of detection of incidental findings. A prospective study by Swensen *et al*. [100], including 1520 high-risk individuals who underwent lung cancer screening with low-dose CT found significant, non-pulmonary incidental findings in 14% of the participants. The need for optimization of imaging resources and radiation exposure raises the question whether there is a cost-effective, low-dose alternative to CT in detection and characterization of pulmonary nodules.

Magnetic Resonance Imaging

MRI is a non-ionizing modality, and a study by Cieszanowski *et al.* [101] found detection rates of 75% for CT-proven nodules 4-6 mm, 87.5% for nodules 6-8 mm and 100% for nodules >8 mm and a good agreement between maximum nodule diameter on CT and MRI. CT measurements were however performed on images with a slice thickness of 3 mm, where recommended thickness is ≤1.5 mm [80]. Schroeder *et al.* [102] found a sensitivity for MRI protocols with a Half-Fourier Acquisition Single-shot Turbo spin Echo (HASTE) sequence of 86.3% for nodules 3-5 mm, 95.7% for nodules 6-10 mm and 100% for nodules >10 mm.

Positron-Emission Tomography and Computed Tomography

PET provides important information on cell glucose metabolism, which is elevated in many malignant conditions, and the examination is combined with CT for adequate anatomical orientation. PET-CT is to be considered for indeterminate nodules >8 mm or 250 mm^3 and for nodules with an estimated risk of malignancy >10% [76, 85]. The PET signal is dependent on the size and cell density of a lesion, and examination of subsolid nodules and small solid nodules with diameter under the spatial resolution of the system (approximately 6-10 mm) might lead to false negative findings. PET uptake is unspecific and cannot be used to rule out disease; low-grade lung tumors such

as carcinoid and some adenocarcinomas can have low or normal glucose metabolism, and non-malignant, nodular conditions caused by infection or inflammation such as sarcoidosis can present with very high FDG uptake.

Digital Tomosynthesis

DTS is superior to CXR in depiction of small solid nodules [33, 103], and has been suggested as a low-dose alternative to CT for lung cancer screening [19]. Terzi *et al.* [104] found detection rates of noncalcified nodules in DTS comparable to low-dose CT in a lung cancer screening cohort, but CT was performed only in cases with positive findings on DTS. Other studies have reported detection rates of CT-proven nodules between 56 and 70% [31, 105-107]. Detection rates of ground-glass opacity nodules in DTS is comparable to CXR and inferior to CT, and DTS is consequently not recommended as imaging modality for subsolid nodular lesions [108].

The majority of studies comparing DTS and CT are however based on individuals admitted to CT due to suspicion of disease, and the current knowledge regarding the performance of DTS in detection, characterization and follow-up of incidental nodules is limited [109].

2.4 RADIATION EXPOSURE IN MEDICAL IMAGING

HEALTH CONSIDERATIONS

There are two main health concerns of radiation [110]. The deterministic effects involve tissue damage at radiation doses over a certain threshold such as skin erythema, hair loss or fetal abnormality, and the severity is related to the degree of radiation exposure. The stochastic effects are malignant transformation of cells, with a linear no-threshold relation between radiation exposure and risk for cancer. Whether there is a "safe" amount of radiation regarding stochastic effects is a debated issue [110-112].

The environment is the main source of ionizing radiation, and the amount is dependent on factors such as altitude, levels of radon in the ground, type of construction of houses and transport by airline. Radiation exposure from medical imaging can be considerable for patients undergoing repeated examinations or radiation therapy. Special consideration should therefore be taken in imaging of young people, who are more vulnerable to radiation exposure and have a long expected lifetime, where potential radiation-induced malignancies can become symptomatic. The ALARA, "As low as reasonably achievable" principle states that all medical images should be of sufficient diagnostic quality, achieved at radiation doses as low as possible [113].

ESTIMATION OF RADIATION EXPOSURE

Health risks associated with medical imaging are often quantified in terms of effective dose, a mathematical estimate that include a weighting factor for the assumed sensitivity of the radiated area, but the estimate does not account for any patient-specific risk factors. The ICRP publication 103 [114] states that effective dose should be used for planning and optimization of radiological examinations and procedures, but not for estimation of exposure and risk on individual level. Estimation of effective dose is based on the *absorbed dose*, which is the amount of energy given per mass unit, expressed as gray (Gy) and 1Gy = 1 joule (J)/kg tissue. Equivalent dose is the sum of absorbed dose multiplied with weight factors for the different types of radiation exposure, where x-ray has a factor of 1.0, the unit of the product is J kg^{-1}, and 1 J kg^{-1} equals 1 Sievert (Sv). Equivalent dose is an estimate of the degree of potential damage in the exposed tissue, with cumulative and stochastic effects regarding risk of radiation-induced cancer

DOSE ESTIMATES IN CT

CT is the main source of radiation exposure from diagnostic imaging [115]. The CT scan report includes the computed tomography dose index (CTDI) (mGy), when accounted for pitch expressed as $CTDI_{vol}$, which is an estimate of the average absorbed dose in the scanned volume based on calculations on a phantom. The dose-length product (DLP) is the product of the computed tomography dose index $(CTDI)_{vol}$ and total scan length, and represent an estimate of the total amount of radiation exposure, often expressed in $mGycm^{-1}$. Effective dose is estimated by multiplying the DLP by a conversion factor ($mSv \cdot mGy^{-1} \cdot cm^{-1}$), providing a theoretical dose that takes the estimated average sensitivity of the radiated tissues into account. The chest is the body part with the highest conversion factor for adult women (0.0185 at 120 kVp), and the second highest (0.0105 at 120 kVp) for men [116]. The head has the lowest conversion factor for both children and adults, even though more recent studies have shown a considerable sensitivity of the eye lens [117].

DOSE ESTIMATES IN DTS

Radiation exposure in DTS can be estimated by a method developed by Båth *et al.* [118]. The dose-area-product (DAP) is calculated based on values stored in the scout image, and effective dose is estimated by multiplying the DAP value with a conversion factor of 0.26 $mSv\ Gy^{-1}cm^{-2}$ for the standard 70 kg patient [119]. This method provides a slight overestimation of effective dose in patients with greater BMI than the standard patient, and an underestimation in smaller patients. Adjusted weight factors was therefore proposed by Svalkvist *et al.* [120].

3 AIMS

This thesis is part of a larger project with the aim to evaluate the clinical usefulness of chest tomosynthesis, and the overarching hypothesis is that chest tomosynthesis can be a low-dose alternative to CT in imaging of the lungs. The hypothesis was tested by examining the performance of chest tomosynthesis in comparison to CT in four studies addressing the following specific aims:

I. To investigate visibility of anatomical structures in patients with cystic fibrosis, and the dependency on location and observer experience (Paper I).

II. To investigate assessment, quantification and surveillance of CF-related pulmonary pathology (Paper II).

III. To investigate detection and characterization of incidental indeterminate solid pulmonary nodules (Paper III).

IV. To investigate the determination of size and monitoring of size changes in indeterminate solid pulmonary nodules (Paper IV).

4 MATERIALS AND METHODS

4.1 PATIENT MATERIAL

CYSTIC FIBROSIS (PAPERS I AND II)

Papers I and II are prospective studies involving consecutively invited adult patients followed at the CF-center at Sahlgrenska University Hospital, who undergo triannual surveillance with CT and lung function test. Participants were examined in the period between March 2011 and February 2017. The studies involved an additional DTS in conjunction to the standard follow-up CT. The Regional Ethical Review Board approved the studies, which were performed in accordance to the World Medical Association Declaration of Helsinki [121], with oral and written informed consent obtained from all participants.

The inclusion criterion for Paper I was helical CT and DTS performed on the same day in the period from March 2011 to February 2014. A total of 50 patients underwent follow-up in this period, and 21 fulfilled the criteria for inclusion. The inclusion criteria for Paper II was transaxial or helical CT and DTS performed on the same day at two occasions at the planned triannual follow-up, and 31 patients fulfilled this criteria. The main reason for not fulfilling the criterion for inclusion was incomplete imaging (CT+DTS) on the same day for both studies. A participant flowchart for Paper I and II is presented in Figure 11.

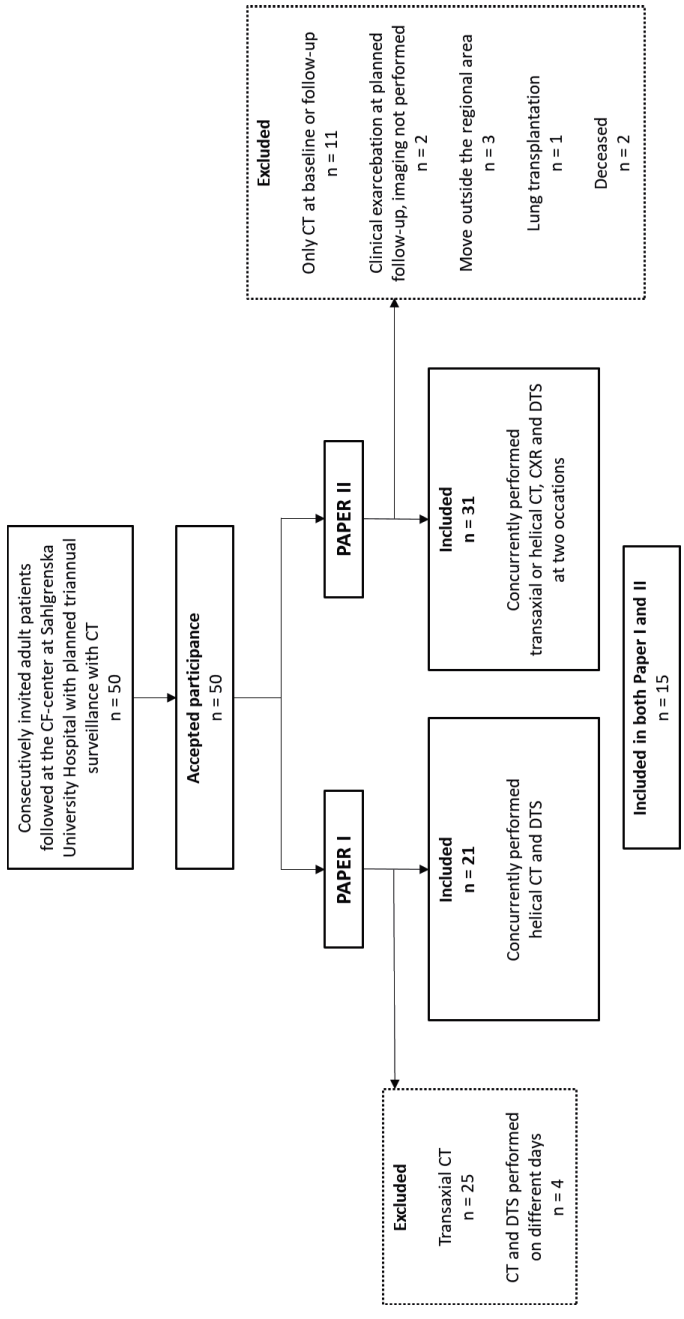

Figure 11. Participant flowchart for Papers I and II.

SOLID PULMONARY NODULES (PAPERS III AND IV)

Papers III and IV are prospective, observational studies with participants recruited from the pilot study of the Swedish CArdioPulmonary bioImage Study (SCAPIS) [122]. The overall aim of SCAPIS is to predict and prevent cardiovascular disease and chronic obstructive pulmonary disease, and participants in the pilot trial underwent an extensive medical examination, including functional tests, blood samples and diagnostic imaging. The pilot SCAPIS was conducted at Sahlgrenska University Hospital between February and November 2012, and the 1111 participants were randomly invited from the Swedish population registry stratified by socioeconomic resident areas. Criteria for inclusion were aged 50-64 year, and the ability to understand Swedish in written and spoken form. Incidental, solid nodules fulfilling the regional guidelines for follow-up, based on the 2005 guidelines from the Fleischner Society [88], were identified in 149/1111 (13.4%) of the participants. These were invited to an additional study, which included DTS in conjunction to the standard follow-up CT at approximately 6, 12 and 24 months after nodule detection. The studies was approved by Regional Ethical Review Board and were performed in accordance to the World Medical Association Declaration of Helsinki [121], with oral and written informed consent obtained from all participants. A flowchart for Papers III and IV is presented in Figure 12.

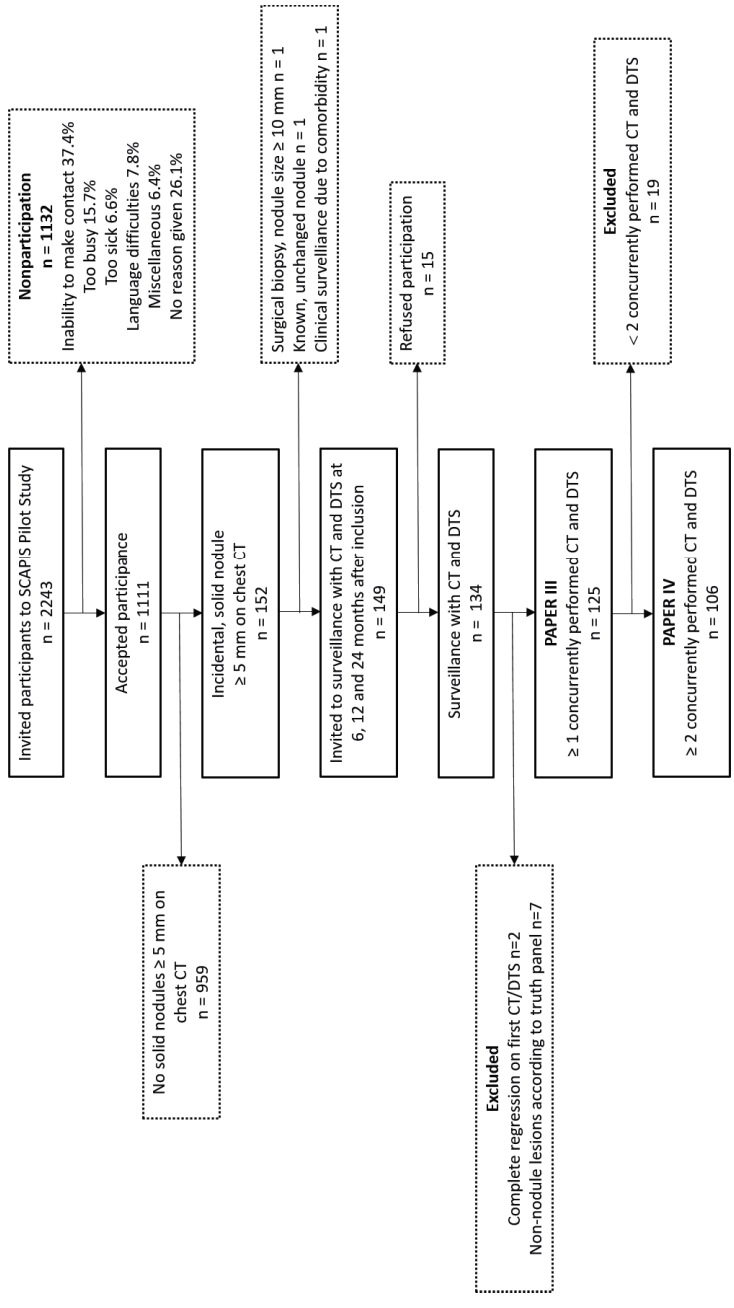

Figure 12. Participant flowchart Papers III and IV.

4.2 IMAGE ACQUISITION AND ESTIMATION OF RADIATION DOSE

All planned imaging modalities included in Papers I-IV were performed on the same day in order to give the best possible conditions for comparison. DTS was performed in addition to the standard CT and CXR examinations. No repeated examinations were allowed due to radiation considerations.

CXR AND DTS PAPERS I-IV

All examinations were performed with the commercially available GE Definium 8000 or GE Discovery XR656 with the VolumeRAD option (GE Healthcare, Chalfont St Giles, UK). A frontal and a lateral radiograph was obtained in standing position, and the frontal image was used as a scout for the DTS. Sixty low-dose projection radiographs were thereafter acquired during approximately 10-second of breath hold at full inspiration. The tube performed a standard caudocranial movement -15° to +15° relative to the standard AP direction at a tube voltage of 120kV, which has been suggested as optimal for DTS of the chest [123]. The low-dose projections were reconstructed to approximately 60 coronal section images with a reconstruction interval of 5 mm.

CT IN CYSTIC FIBROSIS (PAPERS I AND II)

The studies of patients with cystic fibrosis were performed in a transition time between transaxial CT and low-dose helical CT as standard imaging modality. The first examinations included in Paper II were mainly with transaxial HRCT technique, and 4/31 participants were examined by transaxial HRCT on both baseline and follow-up during the study period between 2011 and 2017. There was no definition of a specific study CT scanner, and examinations were performed at eight different machines, and 2/31 patients in Paper II were examined by the same machine and protocol on baseline and follow-up. Paper I included only helical CT for better localization and comparison in DTS of predefined structures in CT images. Included images were acquired in supine or prone position at maximal inspiration and expiration without intravenous contrast media.

CT IN PULMONARY NODULES (PAPERS III AND IV)

Imaging in the SCAPIS pilot study was performed with a Somatom Definition Flash Dual Source (Siemens Healthineers, Forcheim, Germany) CT scanner designated to research. All patients were examined in supine position with arms above head during inspiration. Imaging parameters were: tube voltage of 120 kV, automatic current modulation (CARE Dose 4D with reference mAs 25-30), rotation time 0.5 s and pitch 0.9-1.2. Standard reconstruction algorithms were B31f with a slice thickness of 0.6 mm.

ESTIMATION OF RADIATION DOSE

The effective dose for CT was estimated by multiplying the DLP by the conversion factor of 0.017 $mSvGy^{-1}cm^{-1}$, as recommended by European Guidelines [116]. Effective dose for DTS was estimated for the 70 kg standard patient by multiplying the dose-area product (DAP) by 0.26 $mSvGy^{-1}cm^{-2}$ [119]. DAP was calculated from data in the digital imaging and communications in medicine (DICOM) header of the scout image [118]. Paper III included an additional body mass index-adjusted estimate of effective dose in DTS, based on the papers of Båth *et al.* [118] and Svalkvist *et al.* [120].

4.3 ASSESSMENT OF VISIBILITY

All examinations were anonymized and all studies involved assessment of image quality and the possibility to rate a lesion as inadequately visualized for assessment.

CYSTIC FIBROSIS

Paper 1

Visibility of specific anatomical structures at DTS was assessed by a head-to-head comparison to CT. The specific structures of interest were marked with a circle in transverse CT images, and the task for the observer was to locate the corresponding structure in DTS, and independently rate the visibility compared to CT on a scale from 0 to 5. The observers were chosen in order to assess differences of perceived visibility according to experience, having one pulmonologist, one resident radiologist and one experienced thoracic radiologist as observers.

Paper 2

Quantification of structural, pathological changes over time was estimated by modality-specific scoring systems for CF including the Vult von Steyern (VvS) score [49] for DTS, CF-CT score [58] for CT and Northern score [68] for CXR. Observers with expert knowledge in the respective scoring method independently scored the examinations in a randomized order. Inter- and intraobserver data were achieved by a re-scoring of a subset of 25 randomly selected cases.

PULMONARY NODULES

Paper III

Suspected lung nodules in DTS were marked and characterized by four thoracic radiologists who independently read the examinations in a randomized order. Each marking was rated regarding the confidence of presence of a nodule, as 1, probably not; 2, possibly; 3, probably; 4, definitely a nodule). Each marking was also assessed regarding confidence of recommendation for follow-up, as 1, definitely not; 2, probably not; 3, indeterminate; 4, probably; and 5, definitely.

Paper IV

Solid nodules, marked with a circle in DTS images from baseline and follow-up were independently measured by two thoracic radiologists in a randomized order. The observers were also asked to make a "clinical assessment" of size change between the two examinations, as either decreased, unchanged or increased in size. An interobserver analysis in DTS was performed by re-reading of all cases by one of the observers in a new, randomized order. Semi-automated volume estimates on CT was performed by third observer, and 30 randomly chosen cases was independently re-analyzed by a fourth observer.

4.4 SOFTWARE FOR OBSERVATIONAL STUDIES - VIEWDEX

Observational studies are preferable performed in a standardized setting, with anonymized images displayed in a randomized order. ViewDEX [124, 125] is a specially designed software for observational studies, which allows marking, measurements and scoring of structures of interest. Each marking is logged with coordinates, which enables analysis regarding lesion localization and non-lesion localization, which can be further analyzed with methods such as JAckknife Free-response Receiver Operating Characteristics, further described in the next section. The system also enables definition of structures of interest in the images, for example around a specific nodule in a measurement study. An example of a study setup in ViewDEX is presented in Figure 13.

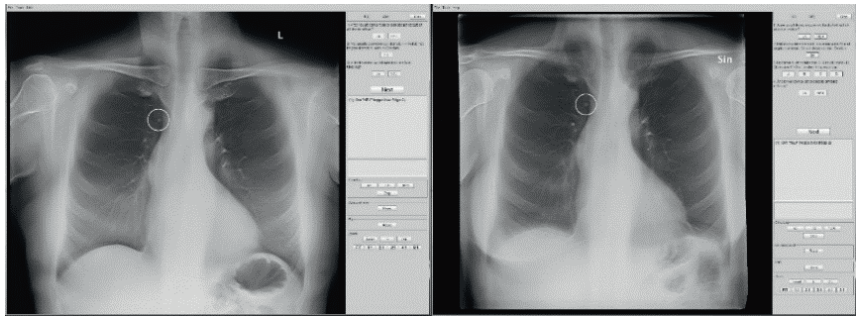

Figure 13. Illustration of an observation study of baseline DTS (left) and follow-up DTS (right) displayed in ViewDEX. The nodule of interest is pre-marked with a circle.

5. STATISTICAL METHODS

Observer studies are central in the validation of a new modality, and the type of data requires specific statistical methods for comparison and generalization of the results [126].

VISUAL GRADING CHARACTERISTICS

Visibility can be analyzed using visual grading characteristics (VGC) [127], which is a method for observational studies with ordinal data, such as a visibility score. The values and range of a rating scale will be used differently for each observer, and the VGC method describes the relationship between two sets of data and not the absolute value of the scores. The result is a VGC curve, which is based on a plot of the proportion of ratings above a certain threshold for one set of data, against another set of data, at various threshold settings. The area under the curve is a value between 0 and 1, and 0.5 represents equality between the two data sets, describing for example perceived visibility between observers, or between anatomical locations for a given observer. The random-reader analysis available in the VGC Analyzer [128] enables a generalization of the results to a population of observers. VGC was used to analyze differences in perceived visibility between observers, and between different anatomical locations for a given observer in Paper I.

RECEIVER OPERATING CHARACTERISTICS

Receiver Operating Characteristics (ROC) statistics [129] was developed in Britain during World War II as a method of assessing the ability to differentiate signals from true danger (enemy aircraft) from harmless objects such as birds, among radar receiver operators. The method has been developed ever since and is now commonly used for evaluation of the performance in medical imaging. A ROC curve is based on data from false- and true positive observations, and false- and true negative markings, plotting the sensitivity of the modality on the y-axis, against 1-specificity on the x-axis. The resulting area under the curve (AUC) is an estimate of the accuracy of the test, and the probability that a true-positive finding will receive a higher score than a false-positive finding. An AUC of 1 represents a test with 100% sensitivity and specificity, while an AUC of 0.5 corresponds to performance equal to chance.

The modified ROC analysis DBM MRMC [130] allows analysis based on multiple readers and cases. ROC analysis was used to estimate the ability to distinguish nodules fulfilling the criterion for follow-up from smaller nodules in Paper III, and in Paper IV for the performance of DTS to detect change in nodule size on CT.

JACKKNIFE FREE-RESPONSE RECEIVER OPERATING CHARACTERISTICS

JAckknife Free-response Receiver Operating Characteristics (JAFROC) [131] is a development of ROC, which is designed for tasks where the localization of a lesion must be taken into account. The method is based on both marking and rating of the structure of interest, and each case can have an unrestricted number of markings and ratings. The analysis can be performed on case level or lesion level, and analysis on lesion level takes the effect of clustered data into account. JAFROC is further available in the JAFROC and JAFROC1 version, where the latter also includes data from non-lesion localizations (false positive markings). The result of the analysis is a figure-of-merit (FOM), which represents the probability that a true-positive finding (lesion localization), is rated higher than a structure of another origin (non-lesion localization). JAFROC analysis was applied in Paper III to assess the performance of nodule detection in DTS.

ASSESSING AGREEMENT

Estimate of inter- and intraobserver agreement is difficult but important for generalization of the results. The number of observations and the distribution within the given categories affect agreement, and agreement by change should be accounted for.

Cohen's kappa [132] is a common method for assessment of reproducibility (do we receive the same result for another observer in a setting with identical circumstances?), and repeatability (does the same observer obtain the same result in a re-reading under identical circumstances?). The analysis describes the agreement between two observations after correction of the expected agreement by chance. A kappa value $\kappa = 1$ indicates perfect agreement, $\kappa = 0$ represent an agreement equal to that by chance, and $\kappa < 0$ is agreement inferior to that by chance. There are suggested levels of agreement for κ values between 0 and 1, but these should be used with caution, and can only be calculated and

compared between observations within the same material and conditions. Cohen's kappa is available in different versions depending on the type of data. The weighted version can be applied to ordered data and takes the level of disagreement into account, whereas the unweighted version puts equal weight to any degree of disagreement. Linear weights are preferred when the distance between each scale step is equally important, and quadratic weights are applied when the relationship between the categories is unequal or non-ordinal. A main disadvantage of the weighted Cohen's kappa is that it only allows comparison of two observations. Cohens's kappa was used in Paper III for assessment of inter- and intraobserver agreement regarding detection and recommendation for follow-up of pulmonary nodules.

The *Krippendorff's alpha* [133, 134] can be applied to any type of data, including ordinal data with multiple observers, and can handle cases with missing data. The coefficient is an estimate of $(De - Do)/De$, where *Do* is the observed disagreement and *De* the estimate of the disagreement by chance. Krippendorff's alpha is available in an unweighted and a weighted version, the latter recommended for ordinal data. The main advantages of Krippendorff's alpha are that it can be applied to ordinal data, that all assessments with minimum two observations are included in the analysis, and that the actual sample size is taken into account [135]. Krippendorff's alpha was used in Paper II for estimation of intra- and interobserver reliability regarding quantitative assessment of extent of CF disease.

A *Bland-Altman plot* [136] illustrates the agreement between two sets of measurements of the same parameter, without the need to define the reference "true" value. The difference between the two measurements on the y-axis plotted against the mean of the two measurements on the x-axis allows identification of systematic differences between the measurements. The 95% confidence interval (CI) of the mean difference between the methods is used to assess any significant systematic differences between the two measurements. The 95% limits of agreement (LOA), calculated as mean difference ±1.96 standard deviations (SD) of the difference, reflects the expected range of difference between the modalities for 95% of the observations. The LOA can be misleadingly wide for small sample sizes, and the 95% CI of the LOA should be taken into account. Analysis according to Bland-Altman was used in Paper I for comparison of lung volume on DTS and CT, and in Paper IV for assessment of intra-, interobserver and intermodality differences in estimation of nodule size and change in size on DTS and CT.

ASSESSING CORRELATION

Correlation analysis describes the degree of association between two variables, and can be assessed with Spearman's and Pearson correlation coefficient [137]. The Pearson correlation coefficient can be applied to continuous pairs of data with an assumed linear relationship, and the absence of outliers. A line which best describes the relationship is drawn through the midst of the points in a scatter plot. The correlation coefficient describes the spread of the observation from that line, where -1 and 1 is perfect correlation (no spread), and 0 suggests no linear relation between the measurements. The Spearman's rank correlation coefficient can be applied to ordinal data with a non-linear relationship. The method applies a monotonic relation, which means that all x-values should have a higher corresponding y-value than any lower x-value. A Spearman's rank correlation value of 1 indicates perfect correlation. Spearman's rank correlation was used in Paper II for assessment of intermodality correlation regarding scores for extent of CF disease.

CLUSTERED DATA

Most studies involve patients followed at the same hospital, with multiple observations in each patient, assessed by more than one observer. The different observations are often positively correlated, and results will be biased if the effect of clustered data is not taken into account. Both the sensitivity and specificity of the test can be effected, and especially the standard error and confidence interval of the estimates. The "true" sample size will be overestimated in multiple observations in the same patient or by the same observer, and the more important "effective" sample size refers to the number of independent observations. The effect of clustered data can be minimized in the study setup by reducing the number of observers and allowing only one observation per patient. There are different statistical approaches for adjustment of the effect of clustered data, and the method of choice should be appropriate to the clinical context [138, 139]. Adjustment is also included in some statistical software, such as the JAFROC [140] and MRMC [130] analysis, which were used in Paper III and IV.

ADJUSTMENT FOR MULTIPLE COMPARISONS

Statistical significance is often defined at a p-value ≤ 0.05, with a 5% chance to incorrectly reject the null hypothesis, given that the null hypothesis is true. Multiple comparisons in subsets of data increase the probability for a significant p-value in at least one of the comparisons, and the possibility for an incorrect rejection of the null hypothesis. The effect of multiple comparisons in studies with two groups can be adjusted according to the Bonferroni method [141], where the resulting p-values are multiplied by the number of comparisons, or by adjustment of the definition of significance by dividing the p-value cutoff with the number of comparisons. Bonferroni adjustment was used in Paper II and IV.

6 RESULTS

6.1 CYSTIC FIBROSIS

PAPER I

Mean estimated total lung volume was 0.6 dm^3 liters larger in DTS than CT based on the scout images of both modalities (LoA −0.17 to 1.36 dm^3). Visibility in DTS of anatomical structures in CF patients was reported as equal to CT in 34%, inferior in 52% and superior in 14% of the 1890 visibility ratings from the three observers. Central and peripheral lateral structures had significantly higher ($p \leq 0.001$) ratings in DTS than structures located in the posterior, anterior and basal parts of the lungs. Reported visibility scores were significantly higher for the most experienced observer ($p \leq 0.01$).

The median effective dose was 3.1 mSv (range 1.0-7.2 mSv) for CT and 0.13 mSv (range 0.10-0.16 mSv) for DTS.

PAPER II

The intermodality correlation between total score of extent of CF disease was strong and significant between CXR, DTS and CT, with Spearman's rank correlation coefficients between 0.82 and 0.89 ($p<0.01$). The correlation between DTS and CT was also very strong for bronchiectasis and bronchial wall thickening. ($r = 0.82$-0.91, $p <0.01$). The lowest correlation was for hyperinflation. Intraobserver reliability for total score and subscore was good and comparable for all modalities with $\alpha = 0.62$-0.94, and interobserver reliability was high for total score, bronchiectasis and mucus plugging ($\alpha = 0.83$-0.93) in DTS. The patients were well-managed with relatively stable lungfunction parameters between baseline and follow-up, which impaired the possibility to investigate whether there was a correlation with changes in lung function and DTS score. Intra- and interobserver reliability was calculated with Krippendorff's alpha, with good interobserver reliability for total score, as well as for intraobserver of subscores. The interobserver agreement for some of the subscores showed considerable variation for both DTS and CT.

The median effective dose for baseline examination was 2.7 mSv (range 0.5-10.7 mSv) for CT and 0.14 mSv (range 0.10-0.16 mSv) for DTS. Median effective dose at follow-up was 1.4 mSv (range 0.2-5.0 mSv) for CT and 0.13 mSv (range 0.09-0.16 mSv) for DTS.

6.3 PULMONARY NODULES

PAPER III

The results from the four observers showed DTS detection rates between 48 and 62% of CT-verified solid nodules 5-10 mm in diameter. The JAFROC FOM of 0.47 represents a 47% chance that a true-positive nodule was rated higher than a non-nodule marking in DTS. An ROC AUC of 0.62 regarding recommendation for follow-up represents a 62% probability that a nodule fulfilling the criteria for follow-up received a higher confidence score than a smaller nodule. The interobserver weighted kappa for agreement on confidence for follow-up of nodules 6 mm or larger was 0.43-0.70, and corresponding values for detection of nodules ≥6 mm was between 0.61 and 0.78. A sub-analysis of the false positive markings, previously presented as a scientific poster at the World Congress of Thoracic Imaging, Boston, 2017, showed that 52% of the 125 patients had at least one marking that was incorrectly assessed as a nodule requiring follow-up. Pleural, perifissural, vascular and costal structures were the most common nodule mimics. Examples of nodules mimics are presented in Figures 15-17.

The median effective dose was 1.6 mSv (range 0.4-2.9 mSv) for CT, 0.14 mSv (range 0.09-0.42 mSv) for DTS based on a 70 kg standard patient, and 0.14 mSv (range 0.09-0.30 mSv) for DTS with application of a body mass-index-adjusted conversion factor.

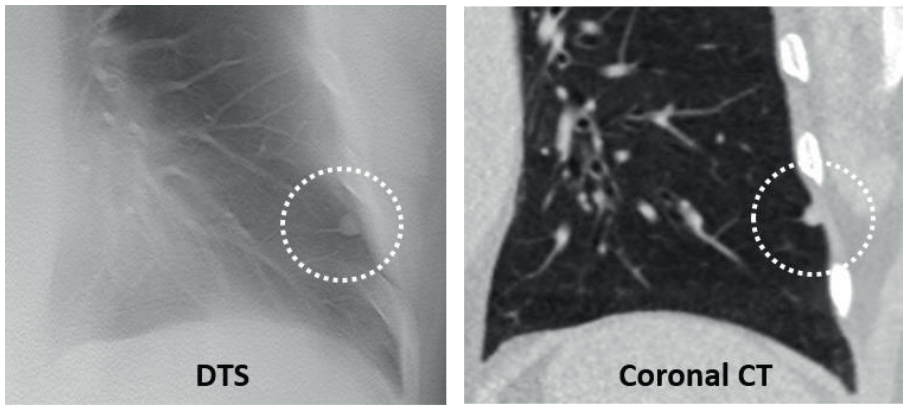

Figure 15. A nodule mimic in DTS. Three out of four thoracic radiologists reported this pleural lesion as "definitely a nodule", and recommended follow-up.

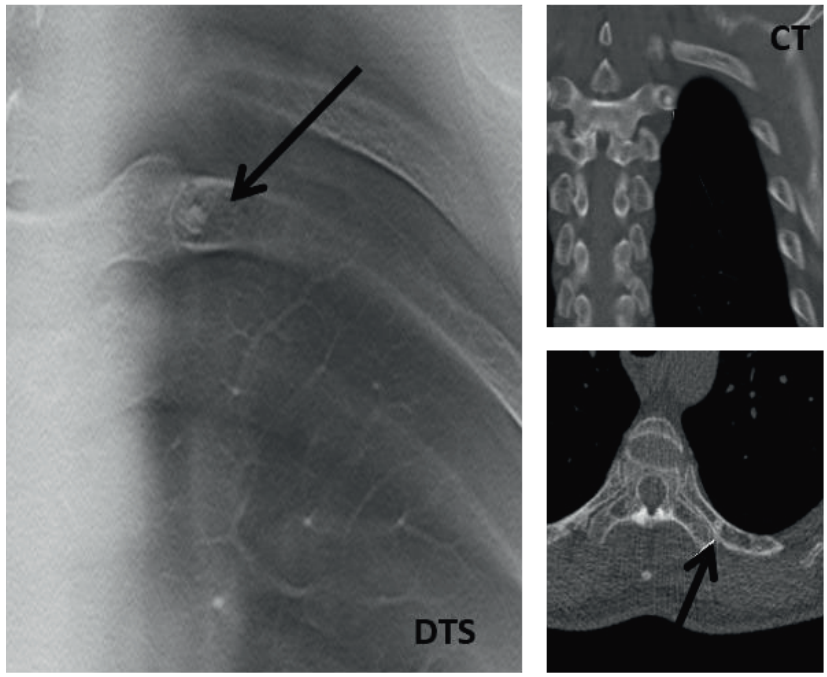

Figure 16. The limited depth resolution of DTS can impair the ability to assess whether a lesion is in, or adjacent to, dense structures. This costal lesion was mistaken as a lung nodule.

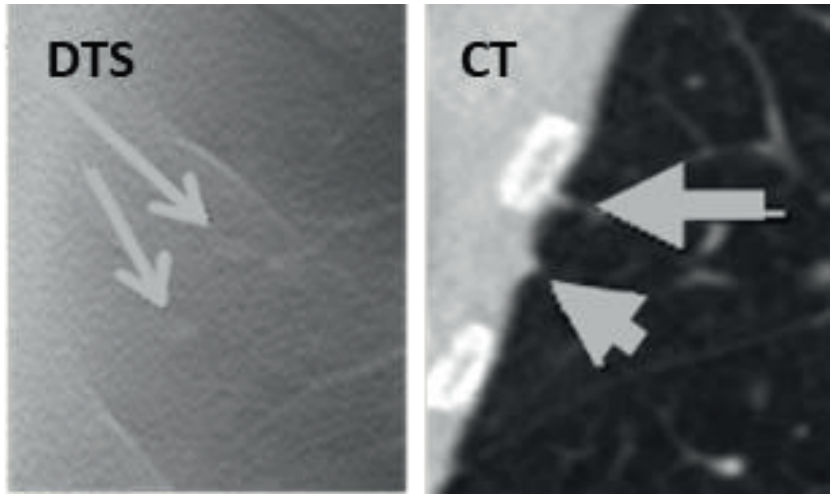

Figure 17. Small, pleural lesions on CT mistaken for intrapulmonary nodules in DTS.

PAPER IV

The ROC AUC curve regarding detection of CT volumetric changes >25% on DTS was 0.58 (CI 0.40-0.76) and 0.50 (CI 0.35-0.66) for observer 1 and 2, respectively. This represents a 58 and 50% chance that a nodule with volumetric change >25% will receive a higher estimated change in size in DTS than a nodule with stable size on CT. The mean difference in change in average, rounded diameter between CT and DTS was -0.14 mm (CI -0.34 to 0.07 mm, SE 0.11 mm, p=0.200, LoA -1.74-1.88 mm) and -0.18 mm (-0.39 to 0.03 mm, SE 0.10 mm, p=0.094, LoA -2.20-1.84 mm) for observers 1 and 2. Histograms are presented in Figure 18. The LoA for difference in volume change between DTS estimates by observer 1 and CT ranged from -39 to 43 mm^3 corresponding to LoA for difference in relative volume change from -58 to 67%.

The median effective dose was 1.6 mSv (range 0.4-7.0 mSv) for CT and 0.15 mSv (range 0.09-0.26 mSv) for DTS.

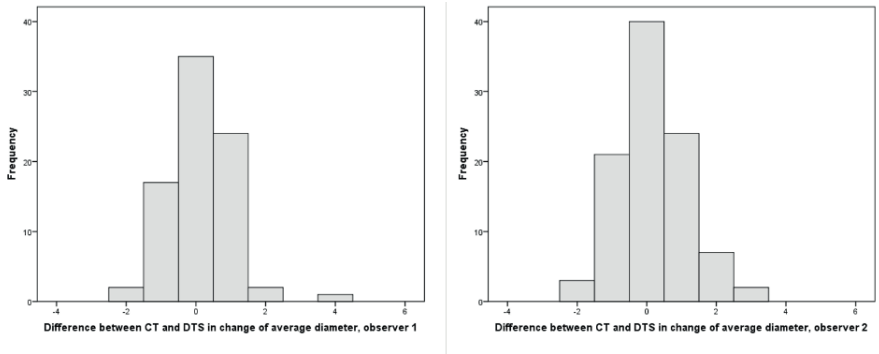

Figure 18. The difference in change of average, rounded diameter between CT and DTS for the two observers.

7 DISCUSSION

7.1 CYSTIC FIBROSIS

Paper I showed that approximately 50% of the visibility ratings of anatomical structures in DTS were in the categories inferior to CT, and that visibility rating was affected by location and observer experience. However, 14% of the ratings were categorized as superior to CT, indicating that the better spatial resolution in DTS could be of importance. Structures adjacent to high-contrast objects such as the ribs in the anterior and posterior part of the lungs received the lowest visibility scores. These areas are more affected by the limited angular movement and consequently a limited depth resolution compared to CT, a well-known limiting factor of DTS [49, 142]. Kim *et al.* [143] investigated the dependency of anatomical location of nodules in a phantom study, and found superior detection of nodules in the paramediastinal and lateral pulmonary regions in DTS compared to CXR and dual-energy subtraction radiography (DES), but similar performance in the retrodiaphragmatic area in accordance with our findings in clinical images.

The effect of observer experience in visibility assessment of CF-related structural changes in DTS has not been previously studied, but there are two available studies regarding imaging of lung nodules. Asplund *et al.* [37] found high performance regarding nodule detection in DTS for inexperienced observers after a short training session, and the results from Lee *et al.* [106] showed high initial performance of nodule detection for inexperienced observers. The results from Paper I showed significantly higher visibility ratings for the most experienced observer.

The results from Paper II showed strong correlation between CXR, DTS and CT in quantification of structural lung disease related to CF. This is, to the knowledge of the author, the first study to compare quantification of pulmonary CF pathology with DTS and CT. The study by Vult von Steyern *et al.* [49] involved comparison to CXR, and Gunnell *et al.* [50] recently compared stationary tomosynthesis with CXR, and both found superior performance in depiction of CF-related pathology with DTS. Choo *et al.* [144] found superior sensitivity and specificity for airway lesions in DTS compared to CXR, with a 94% sensitivity of detection of airway lesions, having CT as reference. The specificity was however comparable between CXR and DTS.

7.2 PULMONARY NODULES

The results from Paper III showed inferior visibility and characterization of CT-verified nodules. Some non-pulmonary lesions were mistaken for nodules requiring follow-up, often related to the limited depth resolution.

Previous studies of nodule depiction in DTS involve mainly comparisons to CXR [31, 33, 107]. The results from the SOS observational study by Terzi and Bertolaccini *et al.* [104, 145] found nodule detection rates comparable to previously reported for CT. However, CT was only performed in cases where a suspected nodule was identified on DTS, which is a clear limitation regarding comparison of the methods. The study by Langer *et al.* [103] and Lee *et al.* [109] are however in line with the results of Paper III, with a detection rate inferior to CT.

Paper IV indicates comparable estimates in size and change in size between manual diameter on DTS and semi-automated diameters on CT. Differences between calculated volume on DTS and volumetric estimates on CT were at a degree of potential clinical impact. The results are in line with the study by Lee *et al.* [109], which found no bias between diameter measurements with DTS compared to CT, and intermodality differences were within the 2 mm cut-off for significant change. However, it has been recommended not to use DTS and CT measurements interchangeably [146].

7.3 EVIDENCE-BASED PRACTICE IN DIAGNOSTIC IMAGING

High quality studies require time for planning, ethical approval, funding and logistical arrangements. The studies included in this thesis were initiated at a time before the availability of ultralow-dose CT, when the median effective dose of routine chest CT was around 8 mSv [112]. Manufacturers of radiological equipment are constantly developing new hardware and software for diagnostic imaging, and it is often not possible to publish studies with the latest available technique at all times. Paper II involved surveillance of CF at two occasions separated by three years, and the time period for examination of all eligible patients at the regional CF center was from March 2011 until January 2017. During this time period there was also a shift toward helical scanning.

However, in the practice of evidence-based medicine, it is important to take the time and effort to evaluate the performance and potential adverse events of a new technique before the introduction in routine clinical practice, which is the aim of this thesis.

Standardized imaging provides methodical strong results, and all DTS examinations in Paper I-IV were performed with equipment from the same manufacturer, with one minor upgrade during the study period. The reference CT examinations in Paper III and IV were correspondingly performed with the same parameters and the same equipment, dedicated for research. However, few hospitals have the resources for such arrangements, and many studies, such as Paper I and II are performed in a clinical environment with the, at the time available equipment.

Many studies involve patients followed at the same hospital, with multiple observations for each patients, assessed by more than one observer. The different observations are often positively correlated, and results will be biased if the effect of clustered data is not taken into account [138]. Both sensitivity and specificity of the test can be effected, and especially the standard error and confidence interval of the estimates. The “true” sample size will be overestimated in multiple observations in the same patient or by the same observer, and the more important “effective” sample size refer to the number of independent observations. The effect of clustered data can be minimized in the study design by allowing only one observation per patient.

7.4 CLINICAL USE OF DTS

The development of low dose CT can question the clinical implications for an additional modality such as DTS. The performance of low-dose and ultra-low-dose CT seems acceptable for visualization and size estimation of solid lung nodules as well as assessment of CF lung disease [7, 8, 147-149], and Yi *et al.* [150] reported acceptable image quality for evaluation of bronchiectasis at tube current settings down to 70 mA with a mean radiation dose of 5.4 mGy. There are possibilities for dose reduction in the order of 50% or more for DTS compared to default settings, without compromising diagnostic performance [123, 151, 152]. Dose optimization of DTS could provide images at a lower dose and higher spatial resolution than ultra-low-dose CT. The results in paper II illustrates the reduction in effective dose during the time span from 2011 to 2017 with a median effective dose 2.7 mSv for CT at first examination and a median effective dose at follow-up of 1.4 mSv.

The availability and cost of CT may vary between and within countries, and can be a limiting factor in health care in many parts of the world. DTS requires less resources in terms of investment in equipment, and both the examination itself, and the reading is less time-consuming than CT [106]. A study by Peterson *et al.* [153] found the potential for DTS as a substitute to CT in 20% of performed examinations during office hours. Thus, the use of DTS in clinical practice could contribute to optimized use of imaging resources. The modality can be used as a problem-solver for inconclusive finding in CXR and as a substitute to CT for selected tasks. DTS can also be used as a high performance alternative to CXR offering improved detection of pathology in areas were CT resources are limited.

8 CONCLUSIONS

The results of the four studies in the present thesis support the hypothesis that chest tomosynthesis can be a low-dose alternative to CT in imaging of the lungs for selected tasks based on the following specific conclusions:

I. Visibility of small anatomical structures in patients with CF is affected by location and inferior to CT particularly in the anterior, posterior and basal regions of the lungs. Perceived visibility varies between observers (Paper I).

II. Assessments of CF-related pulmonary pathology on chest tomosynthesis shows good correlation to assessments on CT in quantification and surveillance of disease affecting the lung parenchyma. (Paper II)

III. Detection and characterization of indeterminate solid nodules is overall inferior to CT although nodules overlooked in CT may be detected in chest tomosynthesis. (Paper III).

IV. Determining size as well as monitoring size changes in indeterminate solid lung nodules is feasible in chest tomosynthesis when applying diametrical measurements. (Paper IV)

9 FUTURE PERSPECTIVES

A radiation dose equal to CXR would increase the use of DTS in routine clinical practice, with a higher performance at no additional risk of radiation-induced disease. Lee *et al.* [154] recently evaluated the technique of deep convolutional neural networks to generate high-quality images from low-dose DTS images. They obtained a reduction in effective dose from 0.89 mSv to 0.11 mSv, with comparable image quality as standard DTS. However, the reduced dose is comparable to the dose of the standard dose DTS examinations included in this thesis. Training and development of the technique might enable further dose reduction in DTS, possibly to the level of CXR.

The purpose of surveillance of indeterminate nodules is to identify early, localized and curable cancer. The most sensitive method has been calculation of VDT based on change in volumetric estimates on CT [85]. Radiomic analysis is a hot topic in diagnostic imaging, with a potential for nodule characterization on initial CT. Yunlang *et al.* [155] found radiomics features helpful in differentiation between indolent and invasive lung adenocarcinomas, and several other studies support the value of the method in the assessment of inderminate nodules [156-159].

One could speculate that the improved spatial resolution of DTS in comparison to CT might provide new radiomics to be used in artificial intelligence driven multiparametric decision support systems for healthcare.

10 ACKNOWLEDGEMENTS

This study was financed by grants from the Swedish state under the agreement between the Swedish government and the county councils, the ALF-agreement, the Swedish Research Council and Department of Radiology, Oslo University Hospital, Norway.

First, I would like to thank the patients at the Gothenburg CF-center and participants in the SCAPIS pilot study for proving us with material for clinical validation of a new modality.

This thesis is the result of a wonderful effort from dedicated researchers, clinicians, colleagues, family and friends. There are many contributors, and among these;

Åse Allansdotter Johnsson, my outstanding principal supervisor. It has been a great honor to be your first PhD student. Besides, from being a mentor in the scientific work, you have also been a tremendous support in all aspects of being a PhD student, telling me to slow down and take a breath at times of intense work. I could not imagine a better supervisor than you, and you have become a very dear friend.

Jenny Vikgren, my very wise co-supervisor. I admire your sense of working hard. You have a wonderful way to look at things from a perspective, and your expertise in both research and thoracic imaging has been invaluable in this thesis. It is inspiring how you always find the time for research in a very busy schedule.

Magnus Båth, my hardworking co-supervisor with an impressive scientific career. Your broad knowledge in physics and statistics have forced me to learn many things that I would otherwise probably ask someone else to do. I am very grateful to have achieved the skills to perform the statistics included in this thesis, as well as an understanding of the physical aspects of diagnostic imaging.

The wonderful physicists; Maral Mirzai Beni, Angelica Svalkvist and Christina Söderman, for guidance regarding ViewDEX, imaging parameters, radiation dose and statistics, your support has always been just an email away. I believe that a close cooperation between physicists and radiologist is one of the key aspects for scientific work in diagnostic imaging.

Marita Gilljam, your dedication for CF patients is impressive. Thank you for a great cooperation around this patient category, openness to new ideas, clinical and scientific input on manuscripts, and providing clinical data for the study population.

Dear colleagues at Department of Thoracic-, Vascular- and Interventional Radiology, Oslo University Hospital, Ullevål. Combining clinical work, research and family can be challenging, thank you for the support. I will try not to complain about sleepless nights and working weekends any more. I really enjoy sharing interesting cases and time with you.

My family. It has, at times been hard to spend a weekend behind the computer instead of with you. Thank you *Alexander* for all the times you did the wash-up and put the children to bed because of a deadline. Thank you *Nora, Isaac* and *Rakel* for understanding that I was not always mentally available, and most of all for the pleasure of sharing life with you.

Rose. You became part of our family at a time when there was little room for hobbies. Spending time with you, Nora and friends in the stable has been the best way to clear the spirit, and a fantastic cure for stress.

Mum and dad. For always providing a place to eat and sleep when visiting Gothenburg for work. For laid-back conversations after a long day by the computer.

11 REFERENCES

1. Glasser, O., *W. C. Roentgen and the discovery of the Roentgen rays.* AJR Am J Roentgenol, 1995. **165**(5): p. 1033-40.
2. Schaefer-Prokop, C., et al., *Digital chest radiography: an update on modern technology, dose containment and control of image quality.* European radiology, 2008. **18**(9): p. 1818-1830.
3. Richmond, C., *Sir Godfrey Hounsfield.* BMJ : British Medical Journal, 2004. **329**(7467): p. 687-687.
4. Hounsfield, G.N., *The E.M.I. Scanner.* Proceedings of the Royal Society of London. Series B, Biological Sciences, 1977. **195**(1119): p. 281-289.
5. Rubin, G.D., *Computed Tomography: Revolutionizing the Practice of Medicine for 40 Years.* Radiology, 2014. **273**(2S): p. S45-S74.
6. Walsh, S.L. and D.M. Hansell, *High-resolution CT of interstitial lung disease: a continuous evolution.* Semin Respir Crit Care Med, 2014. **35**(1): p. 129-44.
7. Kim, Y., et al., *Ultra-Low-Dose CT of the Thorax Using Iterative Reconstruction: Evaluation of Image Quality and Radiation Dose Reduction.* AJR Am J Roentgenol, 2015. **204**(6): p. 1197-202.
8. Sui, X., et al., *Detection and size measurements of pulmonary nodules in ultra-low-dose CT with iterative reconstruction compared to low dose CT.* Eur J Radiol, 2016. **85**(3): p. 564-70.
9. Som, P., et al., *A fluorinated glucose analog, 2-fluoro-2-deoxy-D-glucose (F-18): nontoxic tracer for rapid tumor detection.* J Nucl Med, 1980. **21**(7): p. 670-5.
10. Townsend, D.W., *Combined positron emission tomography-computed tomography: the historical perspective.* Seminars in ultrasound, CT, and MR, 2008. **29**(4): p. 232-235.
11. Herlin, G., et al., *Role of Scintigraphy with Technetium-99m Depreotide in the Diagnosis and Management of Patients with Suspected Lung Cancer AU - Axelsson, R.* Acta Radiologica, 2008. **49**(3): p. 295-302.
12. Newman, P.G. and G.S. Rozycki, *THE HISTORY OF ULTRASOUND.* Surgical Clinics of North America, 1998. **78**(2): p. 179-195.
13. Yang, J.-x., et al., *Detection of lung atelectasis/consolidation by ultrasound in multiple trauma patients with mechanical ventilation.* Critical Ultrasound Journal, 2009. **1**(1): p. 13-16.
14. Al Deeb, M., et al., *Point-of-care ultrasonography for the diagnosis of acute cardiogenic pulmonary edema in patients presenting with acute dyspnea: a systematic review and meta-analysis.* Acad Emerg Med, 2014. **21**(8): p. 843-52.

15. Currie, S., et al., *Understanding MRI: basic MR physics for physicians.* Postgraduate Medical Journal, 2013. **89**(1050): p. 209-223.
16. Biederer, J., et al., *MRI of the lung (2/3). Why ... when ... how?* Insights into imaging, 2012. **3**(4): p. 355-371.
17. Wild, J.M., et al., *MRI of the lung (1/3): methods.* Insights into imaging, 2012. **3**(4): p. 345-353.
18. Santyr, G., et al., *Hyperpolarized Gas Magnetic Resonance Imaging of Pediatric Cystic Fibrosis Lung Disease.* Academic Radiology.
19. Ferrari, A., et al., *Digital chest tomosynthesis: the 2017 updated review of an emerging application.* Annals of translational medicine, 2018. **6**(5): p. 91-91.
20. Chou, S.-H.S., et al., *Digital Tomosynthesis of the Chest: Current and Emerging Applications.* RadioGraphics, 2014. **34**(2): p. 359-372.
21. Machida, H., et al., *Whole-Body Clinical Applications of Digital Tomosynthesis.* RadioGraphics, 2016. **36**(3): p. 735-750.
22. Skaane, P., *Breast cancer screening with digital breast tomosynthesis.* Breast Cancer, 2017. **24**(1): p. 32-41.
23. Zackrisson, S., *Tomosynthesis in breast screening: great expectations?* The Lancet Oncology.
24. Joo, Y.B., et al., *Digital tomosynthesis as a new diagnostic tool for evaluation of spine damage in patients with ankylosing spondylitis.* Rheumatol Int, 2017. **37**(2): p. 207-212.
25. Ceder, E., et al., *THORACIC SPINE IMAGING: A COMPARISON BETWEEN RADIOGRAPHY AND TOMOSYNTHESIS USING VISUAL GRADING CHARACTERISTICS.* Radiat Prot Dosimetry, 2016. **169**(1-4): p. 204-10.
26. Ha, A.S., et al., *Digital Tomosynthesis to Evaluate Fracture Healing: Prospective Comparison With Radiography and CT.* AJR Am J Roentgenol, 2015. **205**(1): p. 136-41.
27. Ottenin, M.A., et al., *Evaluation of the diagnostic performance of tomosynthesis in fractures of the wrist.* AJR Am J Roentgenol, 2012. **198**(1): p. 180-6.
28. Quaia, E., et al., *Analysis of the impact of digital tomosynthesis on the radiological investigation of patients with suspected pulmonary lesions on chest radiography.* Eur Radiol, 2012. **22**(9): p. 1912-22.
29. Quaia, E., et al., *The Value of Digital Tomosynthesis in the Diagnosis of Suspected Pulmonary Lesions on Chest Radiography.* Academic Radiology. **17**(10): p. 1267-1274.
30. Galea, A., et al., *The value of digital tomosynthesis of the chest as a problem-solving tool for suspected pulmonary nodules and hilar lesions detected on chest radiography.* Eur J Radiol, 2015. **84**(5): p. 1012-8.

31. Vikgren, J., et al., *Comparison of Chest Tomosynthesis and Chest Radiography for Detection of Pulmonary Nodules: Human Observer Study of Clinical Cases.* Radiology, 2008. **249**(3): p. 1034-1041.
32. Kim, E.Y., et al., *Pulmonary Mycobacterial Disease: Diagnostic Performance of Low-Dose Digital Tomosynthesis as Compared with Chest Radiography.* Radiology, 2010. **257**(1): p. 269-277.
33. Dobbins, J.T., 3rd, et al., *Multi-Institutional Evaluation of Digital Tomosynthesis, Dual-Energy Radiography, and Conventional Chest Radiography for the Detection and Management of Pulmonary Nodules.* Radiology, 2016: p. 150497.
34. Bertolaccini, L., A. Viti, and A. Terzi, *Digital tomosynthesis in lung cancer: state of the art.* Ann Transl Med, 2015. **3**(10): p. 139.
35. Chou, S.H., et al., *Digital tomosynthesis of the chest: current and emerging applications.* Radiographics, 2014. **34**(2): p. 359-72.
36. Meltzer, C., et al., *VISIBILITY OF STRUCTURES OF RELEVANCE FOR PATIENTS WITH CYSTIC FIBROSIS IN CHEST TOMOSYNTHESIS: INFLUENCE OF ANATOMICAL LOCATION AND OBSERVER EXPERIENCE.* Radiation Protection Dosimetry, 2016. **169**(1-4): p. 177-187.
37. Asplund, S., et al., *Learning aspects and potential pitfalls regarding detection of pulmonary nodules in chest tomosynthesis and proposed related quality criteria.* Acta Radiol, 2011. **52**(5): p. 503-12.
38. Quaia, E., et al., *The value of digital tomosynthesis in the diagnosis of suspected pulmonary lesions on chest radiography: analysis of diagnostic accuracy and confidence.* Acad Radiol, 2010. **17**(10): p. 1267-74.
39. Stoltz, D.A., D.K. Meyerholz, and M.J. Welsh, *Origins of cystic fibrosis lung disease.* The New England journal of medicine, 2015. **372**(4): p. 351-362.
40. Del Porto, P., et al., *Dysfunctional CFTR alters the bactericidal activity of human macrophages against Pseudomonas aeruginosa.* PloS one, 2011. **6**(5): p. e19970-e19970.
41. Zhang, S., C.L. Shrestha, and B.T. Kopp, *Cystic fibrosis transmembrane conductance regulator (CFTR) modulators have differential effects on cystic fibrosis macrophage function.* Scientific reports, 2018. **8**(1): p. 17066-17066.
42. Keogh, R.H., et al., *Up-to-date and projected estimates of survival for people with cystic fibrosis using baseline characteristics: A longitudinal study using UK patient registry data.* Journal of cystic fibrosis : official journal of the European Cystic Fibrosis Society, 2018. **17**(2): p. 218-227.
43. Castellani, C., et al., *ECFS best practice guidelines: the 2018 revision.* Journal of Cystic Fibrosis, 2018. **17**(2): p. 153-178.
44. Yankaskas, J.R., et al., *Cystic fibrosis adult care: consensus conference report.* Chest, 2004. **125**(1 Suppl): p. 1s-39s.

45. Tiddens, H.A., S.M. Stick, and S. Davis, *Multi-modality monitoring of cystic fibrosis lung disease: the role of chest computed tomography.* Paediatr Respir Rev, 2014. **15**(1): p. 92-7.
46. Tiddens, H.A. and P.A. de Jong, *Imaging and clinical trials in cystic fibrosis.* Proc Am Thorac Soc, 2007. **4**(4): p. 343-6.
47. de Jong, P.A., et al., *Progressive damage on high resolution computed tomography despite stable lung function in cystic fibrosis.* Eur Respir J, 2004. **23**(1): p. 93-7.
48. Biederer, J., et al., *MRI of the lung (3/3)-current applications and future perspectives.* Insights into Imaging, 2012. **3**(4): p. 373-386.
49. Vult von Steyern, K., et al., *Description and validation of a scoring system for tomosynthesis in pulmonary cystic fibrosis.* Eur Radiol, 2012. **22**(12): p. 2718-28.
50. Gunnell, E.T., et al., *Initial clinical evaluation of stationary digital chest tomosynthesis in adult patients with cystic fibrosis.* Eur Radiol, 2019. **29**(4): p. 1665-1673.
51. Hansell, D.M., et al., *Fleischner Society: glossary of terms for thoracic imaging.* Radiology, 2008. **246**(3): p. 697-722.
52. Loeve, M., et al., *Bronchiectasis and pulmonary exacerbations in children and young adults with cystic fibrosis.* Chest, 2011. **140**(1): p. 178-185.
53. van der Bruggen-Bogaarts, B.A., et al., *Screening for bronchiectasis. A comparative study between chest radiography and high-resolution CT.* Chest, 1996. **109**(3): p. 608-11.
54. Sanders, D.B., et al., *The sensitivity of lung disease surrogates in detecting chest CT abnormalities in children with cystic fibrosis.* Pediatric pulmonology, 2012. **47**(6): p. 567-573.
55. Serra, G., et al., *Lung MRI as a possible alternative to CT scan for patients with primary immune deficiencies and increased radiosensitivity.* Chest, 2011. **140**(6): p. 1581-1589.
56. Tepper, L.A., et al., *Validating chest MRI to detect and monitor cystic fibrosis lung disease in a pediatric cohort.* Pediatr Pulmonol, 2016. **51**(1): p. 34-41.
57. Sileo, C., et al., *HRCT and MRI of the lung in children with cystic fibrosis: comparison of different scoring systems.* J Cyst Fibros, 2014. **13**(2): p. 198-204.
58. Brody, A.S., et al., *High-resolution computed tomography in young patients with cystic fibrosis: distribution of abnormalities and correlation with pulmonary function tests.* J Pediatr, 2004. **145**(1): p. 32-8.
59. Eichinger, M., et al., *Morphologic and functional scoring of cystic fibrosis lung disease using MRI.* European Journal of Radiology, 2012. **81**(6): p. 1321-1329.
60. Wielputz, M.O., et al., *Magnetic resonance imaging detects changes in structure and perfusion, and response to therapy in early cystic*

fibrosis lung disease. Am J Respir Crit Care Med, 2014. **189**(8): p. 956-65.
61. Hayden, G.E. and K.W. Wrenn, *Chest radiograph vs. computed tomography scan in the evaluation for pneumonia.* J Emerg Med, 2009. **36**(3): p. 266-70.
62. Eichinger, M., et al., *Contrast-enhanced 3D MRI of lung perfusion in children with cystic fibrosis--initial results.* Eur Radiol, 2006. **16**(10): p. 2147-52.
63. Mentore, K., et al., *Hyperpolarized HHe 3 MRI of the lung in cystic fibrosis: assessment at baseline and after bronchodilator and airway clearance treatment.* Acad Radiol, 2005. **12**(11): p. 1423-9.
64. van Beek, E.J., et al., *Assessment of lung disease in children with cystic fibrosis using hyperpolarized 3-Helium MRI: comparison with Shwachman score, Chrispin-Norman score and spirometry.* Eur Radiol, 2007. **17**(4): p. 1018-24.
65. Chrispin, A.R. and A.P. Norman, *The systematic evaluation of the chest radiograph in cystic fibrosis.* Pediatr Radiol, 1974. **2**(2): p. 101-5.
66. Weatherly, M.R., et al., *Wisconsin cystic fibrosis chest radiograph scoring system.* Pediatrics, 1993. **91**(2): p. 488-95.
67. Brasfield, D., et al., *The chest roentgenogram in cystic fibrosis: a new scoring system.* Pediatrics, 1979. **63**(1): p. 24-9.
68. Conway, S.P., et al., *The chest radiograph in cystic fibrosis: a new scoring system compared with the Chrispin-Norman and Brasfield scores.* Thorax, 1994. **49**(9): p. 860-862.
69. Terheggen-Lagro, S., et al., *Correlation of six different cystic fibrosis chest radiograph scoring systems with clinical parameters.* Pediatr Pulmonol, 2003. **35**(6): p. 441-5.
70. de Jong, P.A. and H.A. Tiddens, *Cystic fibrosis specific computed tomography scoring.* Proc Am Thorac Soc, 2007. **4**(4): p. 338-42.
71. Kongstad, T., et al., *Association between spirometry controlled chest CT scores using computer-animated biofeedback and clinical markers of lung disease in children with cystic fibrosis.* Eur Clin Respir J, 2017. **4**(1): p. 1318027.
72. Rosenow, T., et al., *PRAGMA-CF. A Quantitative Structural Lung Disease Computed Tomography Outcome in Young Children with Cystic Fibrosis.* Am J Respir Crit Care Med, 2015. **191**(10): p. 1158-65.
73. Kuo, W., et al., *Objective airway artery dimensions compared to CT scoring methods assessing structural cystic fibrosis lung disease.* J Cyst Fibros, 2017. **16**(1): p. 116-123.
74. Hammerschlag, G., et al., *Prevalence of incidental pulmonary nodules on computed tomography of the thorax in trauma patients.* Intern Med J, 2015. **45**(6): p. 630-3.

75. Burt, J.R., et al., *Incidental findings on cardiac multidetector row computed tomography among healthy older adults: prevalence and clinical correlates.* Arch Intern Med, 2008. **168**(7): p. 756-61.
76. MacMahon, H., et al., *Guidelines for Management of Incidental Pulmonary Nodules Detected on CT Images: From the Fleischner Society 2017.* Radiology, 2017: p. 161659.
77. de Hoop, B., et al., *Pulmonary perifissural nodules on CT scans: rapid growth is not a predictor of malignancy.* Radiology, 2012. **265**(2): p. 611-6.
78. Ahn, M.I., et al., *Perifissural nodules seen at CT screening for lung cancer.* Radiology, 2010. **254**(3): p. 949-56.
79. Mets, O.M., et al., *Incidental perifissural nodules on routine chest computed tomography: lung cancer or not?* European radiology, 2018. **28**(3): p. 1095-1101.
80. Bankier, A.A., et al., *Recommendations for Measuring Pulmonary Nodules at CT: A Statement from the Fleischner Society.* Radiology, 2017. **285**(2): p. 584-600.
81. Eisenhauer, E.A., et al., *New response evaluation criteria in solid tumours: revised RECIST guideline (version 1.1).* Eur J Cancer, 2009. **45**(2): p. 228-47.
82. Pinsky, P.F., et al., *Performance of Lung-RADS in the National Lung Screening Trial: a retrospective assessment.* Annals of internal medicine, 2015. **162**(7): p. 485-491.
83. McKee, B.J., et al., *Performance of ACR Lung-RADS in a Clinical CT Lung Screening Program.* J Am Coll Radiol, 2016. **13**(2 Suppl): p. R25-9.
84. Revel, M.P., et al., *Are two-dimensional CT measurements of small noncalcified pulmonary nodules reliable?* Radiology, 2004. **231**(2): p. 453-8.
85. Callister, M.E., et al., *British Thoracic Society guidelines for the investigation and management of pulmonary nodules.* Thorax, 2015. **70 Suppl 2**: p. ii1-ii54.
86. Liang, M., et al., *Variation in Screening CT-Detected Nodule Volumetry as a Function of Size.* AJR Am J Roentgenol, 2017. **209**(2): p. 304-308.
87. Goodman, L.R., et al., *Inherent variability of CT lung nodule measurements in vivo using semiautomated volumetric measurements.* AJR Am J Roentgenol, 2006. **186**(4): p. 989-94.
88. MacMahon, H., et al., *Guidelines for management of small pulmonary nodules detected on CT scans: a statement from the Fleischner Society.* Radiology, 2005. **237**(2): p. 395-400.
89. Aberle, D.R., et al., *Reduced lung-cancer mortality with low-dose computed tomographic screening.* N Engl J Med, 2011. **365**(5): p. 395-409.

90. Ru Zhao, Y., et al., *NELSON lung cancer screening study.* Cancer imaging : the official publication of the International Cancer Imaging Society, 2011. **11 Spec No A**(1A): p. S79-S84.
91. McWilliams, A., et al., *Probability of cancer in pulmonary nodules detected on first screening CT.* N Engl J Med, 2013. **369**(10): p. 910-9.
92. Horeweg, N., et al., *Volumetric computed tomography screening for lung cancer: three rounds of the NELSON trial.* Eur Respir J, 2013. **42**(6): p. 1659-67.
93. Mehta, H.J., et al., *The utility of nodule volume in the context of malignancy prediction for small pulmonary nodules.* Chest, 2014. **145**(3): p. 464-472.
94. Heuvelmans, M.A., et al., *Optimisation of volume-doubling time cutoff for fast-growing lung nodules in CT lung cancer screening reduces false-positive referrals.* Eur Radiol, 2013. **23**(7): p. 1836-45.
95. Ko, J.P., et al., *Pulmonary Nodules: growth rate assessment in patients by using serial CT and three-dimensional volumetry.* Radiology, 2012. **262**(2): p. 662-671.
96. Henschke, C.I., et al., *Lung cancers diagnosed at annual CT screening: volume doubling times.* Radiology, 2012. **263**(2): p. 578-83.
97. de Hoop, B., et al., *Screening for lung cancer with digital chest radiography: sensitivity and number of secondary work-up CT examinations.* Radiology, 2010. **255**(2): p. 629-637.
98. Kaneko, M., et al., *Peripheral lung cancer: screening and detection with low-dose spiral CT versus radiography.* Radiology, 1996. **201**(3): p. 798-802.
99. Oken, M.M., et al., *Screening by chest radiograph and lung cancer mortality: the Prostate, Lung, Colorectal, and Ovarian (PLCO) randomized trial.* Jama, 2011. **306**(17): p. 1865-73.
100. SWENSEN, S.J., et al., *Screening for Lung Cancer with Low-Dose Spiral Computed Tomography.* American Journal of Respiratory and Critical Care Medicine, 2002. **165**(4): p. 508-513.
101. Cieszanowski, A., et al., *MR imaging of pulmonary nodules: detection rate and accuracy of size estimation in comparison to computed tomography.* PloS one, 2016. **11**(6): p. e0156272.
102. Schroeder, T., et al., *Detection of Pulmonary Nodules Using a 2D HASTE MR Sequence: Comparison with MDCT.* American Journal of Roentgenology, 2005. **185**(4): p. 979-984.
103. Langer, S.G., et al., *Sensitivity of Thoracic Digital Tomosynthesis (DTS) for the Identification of Lung Nodules.* Journal of digital imaging, 2016. **29**(1): p. 141-147.
104. Bertolaccini, L., et al., *Lung cancer detection with digital chest tomosynthesis: first round results from the SOS observational study.* Ann Transl Med, 2015. **3**(5): p. 67.

105. Dobbins, J.T., et al., *Digital tomosynthesis of the chest for lung nodule detection: Interim sensitivity results from an ongoing NIH-sponsored trial.* Medical Physics, 2008. **35**(6): p. 2554-2557.
106. Lee, K.H., et al., *Digital Tomosynthesis for Evaluating Metastatic Lung Nodules: Nodule Visibility, Learning Curves, and Reading Times.* Korean Journal of Radiology, 2015. **16**(2): p. 430-439.
107. Kim, J.H., et al., *Comparison of digital tomosynthesis and chest radiography for the detection of pulmonary nodules: systematic review and meta-analysis.* Br J Radiol, 2016. **89**(1068): p. 20160421.
108. Doo, K.W., et al., *Comparison of chest radiography, chest digital tomosynthesis and low dose MDCT to detect small ground-glass opacity nodules: an anthropomorphic chest phantom study.* Eur Radiol, 2014. **24**(12): p. 3269-76.
109. Lee, X.W., et al., *Is Digital Tomosynthesis on Par With Computed Tomography for the Detection and Measurement of Pulmonary Nodules?* J Thorac Imaging, 2017. **32**(6): p. W67-w68.
110. Hendee, W.R. and M.K. O'Connor, *Radiation Risks of Medical Imaging: Separating Fact from Fantasy.* Radiology, 2012. **264**(2): p. 312-321.
111. Nguyen, P.K. and J.C. Wu, *Radiation exposure from imaging tests: is there an increased cancer risk?* Expert review of cardiovascular therapy, 2011. **9**(2): p. 177-183.
112. Smith-Bindman, R., et al., *Radiation dose associated with common computed tomography examinations and the associated lifetime attributable risk of cancer.* Archives of internal medicine, 2009. **169**(22): p. 2078-2086.
113. Do, K.-H., *General Principles of Radiation Protection in Fields of Diagnostic Medical Exposure.* Journal of Korean medical science, 2016. **31 Suppl 1**(Suppl 1): p. S6-S9.
114. *The 2007 Recommendations of the International Commission on Radiological Protection. ICRP publication 103.* Ann ICRP, 2007. **37**(2-4): p. 1-332.
115. Fred A. Mettler, J., et al., *Radiologic and Nuclear Medicine Studies in the United States and Worldwide: Frequency, Radiation Dose, and Comparison with Other Radiation Sources—1950–2007.* Radiology, 2009. **253**(2): p. 520-531.
116. Goo, H.W., *CT Radiation Dose Optimization and Estimation: an Update for Radiologists.* Korean J Radiol, 2012. **13**(1): p. 1-11.
117. Shore, R.E., K. Neriishi, and E. Nakashima, *Epidemiological studies of cataract risk at low to moderate radiation doses: (not) seeing is believing.* Radiat Res, 2010. **174**(6): p. 889-94.
118. Bath, M., C. Soderman, and A. Svalkvist, *A simple method to retrospectively estimate patient dose-area product for chest tomosynthesis examinations performed using VolumeRAD.* Med Phys, 2014. **41**(10): p. 101905.

119. Bath, M., et al., *Effective dose to patients from chest examinations with tomosynthesis.* Radiat Prot Dosimetry, 2010. **139**(1-3): p. 153-8.
120. Svalkvist, A., L.G. Mansson, and M. Bath, *Monte Carlo simulations of the dosimetry of chest tomosynthesis.* Radiat Prot Dosimetry, 2010. **139**(1-3): p. 144-52.
121. *World Medical Association Declaration of Helsinki: ethical principles for medical research involving human subjects.* Jama, 2013. **310**(20): p. 2191-4.
122. Bergstrom, G., et al., *The Swedish CArdioPulmonary BioImage Study: objectives and design.* J Intern Med, 2015. **278**(6): p. 645-59.
123. Soderman, C., et al., *Image quality dependency on system configuration and tube voltage in chest tomosynthesis-a visual grading study using an anthropomorphic chest phantom.* Med Phys, 2015. **42**(3): p. 1200-12.
124. Hakansson, M., et al., *VIEWDEX: an efficient and easy-to-use software for observer performance studies.* Radiat Prot Dosimetry, 2010. **139**(1-3): p. 42-51.
125. Svalkvist, A., et al., *VIEWDEX: A STATUS REPORT.* Radiat Prot Dosimetry, 2016. **169**(1-4): p. 38-45.
126. Bath, M., *Evaluating imaging systems: practical applications.* Radiat Prot Dosimetry, 2010. **139**(1-3): p. 26-36.
127. Bath, M. and L.G. Mansson, *Visual grading characteristics (VGC) analysis: a non-parametric rank-invariant statistical method for image quality evaluation.* Br J Radiol, 2007. **80**(951): p. 169-76.
128. Bath, M. and J. Hansson, *VGC ANALYZER: A SOFTWARE FOR STATISTICAL ANALYSIS OF FULLY CROSSED MULTIPLE-READER MULTIPLE-CASE VISUAL GRADING CHARACTERISTICS STUDIES.* Radiat Prot Dosimetry, 2016. **169**(1-4): p. 46-53.
129. Hajian-Tilaki, K., *Receiver Operating Characteristic (ROC) Curve Analysis for Medical Diagnostic Test Evaluation.* Caspian journal of internal medicine, 2013. **4**(2): p. 627-635.
130. Obuchowski, N.A., et al., *Multireader, multicase receiver operating characteristic analysis: an empirical comparison of five methods.* Acad Radiol, 2004. **11**(9): p. 980-95.
131. Chakraborty, D. and H.J. Yoon, *JAFROC analysis revisited: Figure-of-merit considerations for human observer studies*. Vol. 7263. 2009.
132. Cohen, J., *Weighted kappa: nominal scale agreement with provision for scaled disagreement or partial credit.* Psychol Bull, 1968. **70**(4): p. 213-20.
133. Krippendorff, K., *Estimating the Reliability, Systematic Error and Random Error of Interval Data.* Educational and Psychological Measurement, 1970. **30**(1): p. 61-70.

134. Craggs, R., *The Reliability of Multi-Valued Coding of Data AU - Krippendorff, Klaus.* Communication Methods and Measures, 2016. **10**(4): p. 181-198.
135. Zapf, A., et al., *Measuring inter-rater reliability for nominal data - which coefficients and confidence intervals are appropriate?* BMC Med Res Methodol, 2016. **16**: p. 93.
136. Bland, J.M. and D.G. Altman, *Measuring agreement in method comparison studies.* Stat Methods Med Res, 1999. **8**(2): p. 135-60.
137. Mukaka, M.M., *Statistics corner: A guide to appropriate use of correlation coefficient in medical research.* Malawi medical journal : the journal of Medical Association of Malawi, 2012. **24**(3): p. 69-71.
138. Genders, T.S., et al., *Methods for calculating sensitivity and specificity of clustered data: a tutorial.* Radiology, 2012. **265**(3): p. 910-6.
139. Rutter, C.M., *Bootstrap estimation of diagnostic accuracy with patient-clustered data.* Acad Radiol, 2000. **7**(6): p. 413-9.
140. Wagner, R.F., C.E. Metz, and G. Campbell, *Assessment of medical imaging systems and computer aids: a tutorial review.* Acad Radiol, 2007. **14**(6): p. 723-48.
141. Bland, J.M. and D.G. Altman, *Multiple significance tests: the Bonferroni method.* BMJ (Clinical research ed.), 1995. **310**(6973): p. 170-170.
142. Johnsson, A.A., et al., *Overview of two years of clinical experience of chest tomosynthesis at Sahlgrenska University Hospital.* Radiat Prot Dosimetry, 2010. **139**(1-3): p. 124-9.
143. Kim, E.Y., et al., *The advantage of digital tomosynthesis for pulmonary nodule detection concerning influence of nodule location and size: a phantom study.* Clin Radiol, 2017. **72**(9): p. 796.e1-796.e8.
144. Choo, J.Y., et al., *A comparison of digital tomosynthesis and chest radiography in evaluating airway lesions using computed tomography as a reference.* Eur Radiol, 2016. **26**(9): p. 3147-54.
145. Terzi, A., et al., *Lung cancer detection with digital chest tomosynthesis: baseline results from the observational study SOS.* J Thorac Oncol, 2013. **8**(6): p. 685-92.
146. Johnsson, A.A., et al., *Pulmonary nodule size evaluation with chest tomosynthesis.* Radiology, 2012. **265**(1): p. 273-82.
147. Paks, M., et al., *Ultralow dose CT for follow-up of solid pulmonary nodules: A pilot single-center study using Bland-Altman analysis.* Medicine, 2018. **97**(34): p. e12019-e12019.
148. Jin, S., et al., *Lung nodules assessment in ultra-low-dose CT with iterative reconstruction compared to conventional dose CT.* Quantitative imaging in medicine and surgery, 2018. **8**(5): p. 480-490.
149. Loeve, M., et al., *Cystic Fibrosis: Are Volumetric Ultra-Low-Dose Expiratory CT Scans Sufficient for Monitoring Related Lung Disease?* Radiology, 2009. **253**(1): p. 223-229.

150. Yi, C.A., et al., *Multidetector CT of bronchiectasis: effect of radiation dose on image quality.* AJR Am J Roentgenol, 2003. **181**(2): p. 501-5.
151. Hwang, H.S., M.J. Chung, and K.S. Lee, *Digital tomosynthesis of the chest: comparison of patient exposure dose and image quality between standard default setting and low dose setting.* Korean journal of radiology, 2013. **14**(3): p. 525-531.
152. Soderman, C., et al., *EFFECT OF RADIATION DOSE LEVEL ON ACCURACY AND PRECISION OF MANUAL SIZE MEASUREMENTS IN CHEST TOMOSYNTHESIS EVALUATED USING SIMULATED PULMONARY NODULES.* Radiat Prot Dosimetry, 2016. **169**(1-4): p. 188-98.
153. Petersson, C., et al., *AN ANALYSIS OF THE POTENTIAL ROLE OF CHEST TOMOSYNTHESIS IN OPTIMISING IMAGING RESOURCES IN THORACIC RADIOLOGY.* Radiat Prot Dosimetry, 2016. **169**(1-4): p. 165-70.
154. Lee, D. and H.J. Kim, *Restoration of Full Data from Sparse Data in Low-Dose Chest Digital Tomosynthesis Using Deep Convolutional Neural Networks.* J Digit Imaging, 2019. **32**(3): p. 489-498.
155. She, Y., et al., *The predictive value of CT-based radiomics in differentiating indolent from invasive lung adenocarcinoma in patients with pulmonary nodules.* Eur Radiol, 2018. **28**(12): p. 5121-5128.
156. Hawkins, S., et al., *Predicting Malignant Nodules from Screening CT Scans.* J Thorac Oncol, 2016. **11**(12): p. 2120-2128.
157. Hwang, I.P., et al., *Persistent Pure Ground-Glass Nodules Larger Than 5 mm: Differentiation of Invasive Pulmonary Adenocarcinomas From Preinvasive Lesions or Minimally Invasive Adenocarcinomas Using Texture Analysis.* Invest Radiol, 2015. **50**(11): p. 798-804.
158. Chae, H.D., et al., *Computerized texture analysis of persistent part-solid ground-glass nodules: differentiation of preinvasive lesions from invasive pulmonary adenocarcinomas.* Radiology, 2014. **273**(1): p. 285-93.
159. Uthoff, J., et al., *Machine learning approach for distinguishing malignant and benign lung nodules utilizing standardized perinodular parenchymal features from CT.* Medical Physics. **0**(ja).